DE-AR21-96MC33077--01

RECEIVED
DEC 02 1998
OSTI

Tomographic Site Characterization Using CPT, ERT, and GPR

Topical Report
August 1996 - May 1997

By:
Rexford M. Morey

Work Performed Under Contract No.: DE-AR21-96MC33077

For
U.S. Department of Energy
Office of Fossil Energy
Federal Energy Technology Center
P.O. Box 880
Morgantown, West Virginia 26507-0880

By
Applied Research Associates, Inc.
120-A Waterman Road
South Royalton, Vermont 05068

Disclaimer

This report was prepared as an account of work sponsored by an agency of the United States Government. Neither the United States Government nor any agency thereof, nor any of their employees, makes any warranty, express or implied, or assumes any legal liability or responsibility for the accuracy, completeness, or usefulness of any information, apparatus, product, or process disclosed, or represents that its use would not infringe privately owed rights. Reference herein to any specific commercial product, process, or service by trade name, trademark, manufacturer, or otherwise does not necessarily constitute or imply its endorsement, recommendation, or favoring by the United States Government or any agency thereof. The views and opinions of authors expressed herein do not necessarily state or reflect those of the United States Government or any agency thereof.

DISCLAIMER

Portions of this document may be illegible in electronic image products. Images are produced from the best available original document.

SUMMARY

The U.S. Department of Energy (DOE) is responsible for the cleanup of inactive DOE sites and for bringing DOE sites and facilities into compliance with federal, state and local laws and regulations. The DOE's Office of Environmental Management (EM) needs advanced technologies that can make environmental restoration and waste management operations more efficient and less costly. These techniques are required to better characterize the physical, hydrogeological, and chemical properties of the subsurface while minimizing and optimizing the use of boreholes and monitoring wells. Today the cone penetrometer technique (CPT) is demonstrating the value of a minimally invasive deployment system for site characterization.

Applied Research Associates is developing two new sensor packages for site characterization and monitoring. The two new methods are :

- Electrical Resistivity Tomography (ERT) and
- Ground Penetrating Radar (GPR) Tomography.

These sensor systems are now integrated with the Cone Penetrometer Technique (CPT). The results of this program now make it possible to install ERT and GPR units by CPT methods and thereby reduce installation costs and total costs for ERT and GPR surveys. These two techniques can complement each other in regions of low resistivity where ERT is more effective and regions of high resistivity where GPR is more effective.

The results show that CPT-installed GeoWells can be used for both ERT and GPR borehole tomographic subsurface imaging. These two imaging techniques can be used for environmental site characterization and environmental remediation monitoring. Technologies used for site characterization and monitoring have numerous and diverse applications within site clean-up and waste management operations.

TABLE OF CONTENTS

TABLE OF CONTENTS
(Continued)

LIST OF FIGURES

Section **Page**

LIST OF FIGURES

Section **Page**

LIST OF TABLES

Section **Page**

SECTION I.
INTRODUCTION

The U.S. Department of Energy (DOE) is responsible for the cleanup of inactive DOE sites and for bringing DOE sites and facilities into compliance with federal, state and local laws and regulations. The DOE's Office of Environmental Management (EM) needs advanced technologies that can make environmental restoration and waste management operations more efficient and less costly. Significant savings in both time and money can be realized with better site characterization and monitoring techniques. These techniques are required to better characterize the physical, hydrogeological, and chemical properties of the subsurface while minimizing and optimizing the use of boreholes and monitoring wells. Today the cone penetrometer technique (CPT) is demonstrating the value of a minimally invasive deployment system for site characterization.

ARA's Cone Penetrometer Technique (CPT) uses a variety of sensors for measuring soil properties, such as, pore pressure, resistivity, temperature, pH, and seismic wave speed. Studies have shown that ARA's CPT site investigations at hazardous waste sites are very cost effective when compared to standard drilling methods [1,2]. In its continuing effort to support cost-effective environmental restoration, ARA proposed the development of two new sensor packages for site characterization and monitoring:

- Electrical Resistivity Tomography (ERT), and
- Ground Penetrating Radar (GPR) Tomography.

Cone penetrometer techniques have proven to be an efficient and cost effective method for accessing the subsurface without drilling. ERT and GPR have proven to be useful techniques for imaging of subsurface structures and processes. Past use of ERT and GPR has required the installation of system components via drilled boreholes. The purpose of this project is to make possible the installation of ERT and GPR units by cone penetrometers, reducing installation costs and thereby total costs for ERT and GPR surveys.

The ERT technique uses quasi-dc methods where conduction currents are greater than displacement currents. For most soils the resistivity ranges from 10 to 10^5 ohm-meters and the dielectric constant, which is dictated by the water content, from 4 (dry) to 40 (saturated). In low resistivity conditions, the displacement current (or dielectric effect) is insignificant for frequencies less than 100 kHz. GPR methods, on the other hand, use frequencies from 10 to 1000 MHz where the response is controlled by water content as well as conductivity and where the depth of penetration is limited by attenuation due to low resistivity (high conductivity). Thus, ERT is more effective in *low* resistivity environments and GPR is more effective in *high* resistivity conditions.

Combining the two methods, through an intelligent data fusion process, in a single site characterization survey will greatly enhance the available information about the subsurface conditions at the site.

SECTION II.
PURPOSE

This project addresses a range of DOE problems which fall into two categories: site characterization and monitoring. Technologies used for these purposes have numerous and diverse applications within site clean-up and waste-management operations. DOE has identified a need for sensors, sensor deployment means, and sensor data processing, including sensor data fusion methodologies for:

- Detection and monitoring of contaminants in soils, groundwater, and process effluents
- Expediting site characterization
- Geological and hydrogeological characterization and monitoring of the subsuface environment.

Our project specifically addresses each of these needs:

1. Sensors: ERT and GPR Tomography
2. Sensor Deployment: CPT
3. Sensor Data Processing: Tomographic Imaging
4. Sensor Data Fusion: ERT and GPR

There are numerous specific applications where cost effective underground imaging is very important:

1. Delineating the continuity of soil layers between penetrometer holes
2. Locating and mapping sand and clay lenses between penetrometer holes
3. Mapping DNAPL plumes
4. Defining spatial and temporal behavior of a steam flood for dynamic stripping
5. Detecting leaks under tanks at the DOE's Hanford, WA, site

6. Monitoring the efficiency of air sparging
7. Monitoring an ohmic heating thermal front
8. Characterization of burial trenches and pits, including boundaries and contents
9. *In situ* measurement of physical properties, i. e., porosity, density and moisture content.

SECTION III.
BACKGROUND

This project's goal is to successfully integrate three existing technologies into a successful, cost efficient sensor unit and deployment method. The following describes these three technologies.

A. CONE PENETROMETER TECHNOLOGY

The Cone Penetrometer Test (CPT) was originally developed in the Netherlands in 1934 for geotechnical site investigations. The original cones involved mechanical measurements of the penetration resistance on a conical tip. A friction sleeve was added in 1965 [3]. Electronic measurements were added in 1948 and improved in 1971 [4]. Pore pressure probes were introduced in 1975 [5,6], originally as independent probes, but were soon added to the cone penetrometer instrumentation. These features are illustrated on the CPT probe shown in Figure 1. It contains the primary geotechnical sensors for tip stress, sleeve friction, pore pressure along with an inclinometer to measure the tilt of the probe, and resistivity as discussed later. This type of cone is used widely in Europe for geotechnical investigations. Its acceptance in the United States has been rather limited for geotechnical studies; however, the significant advantages it provides for environmental work are leading to much wider acceptance by the environmental site characterization community. This is due largely to the development of new sensors which allow detection of chemical pollutants in situ.

Major components of the modern cone penetrometer system are the instrumented probe, the instrumentation conditioning and recording system, the hydraulic push system, and the vehicle on which the system is mounted. Enclosure in a van body allows all weather operation. The common configuration provides the reaction mass for a hydraulic push force of about 20 tons (18,000 kgs). Standardization for the geotechnical applications of the cone penetration test was established by the American Society of Testing and Materials in 1986. This standard allows for a probe diameter of 1.44 or 1.75

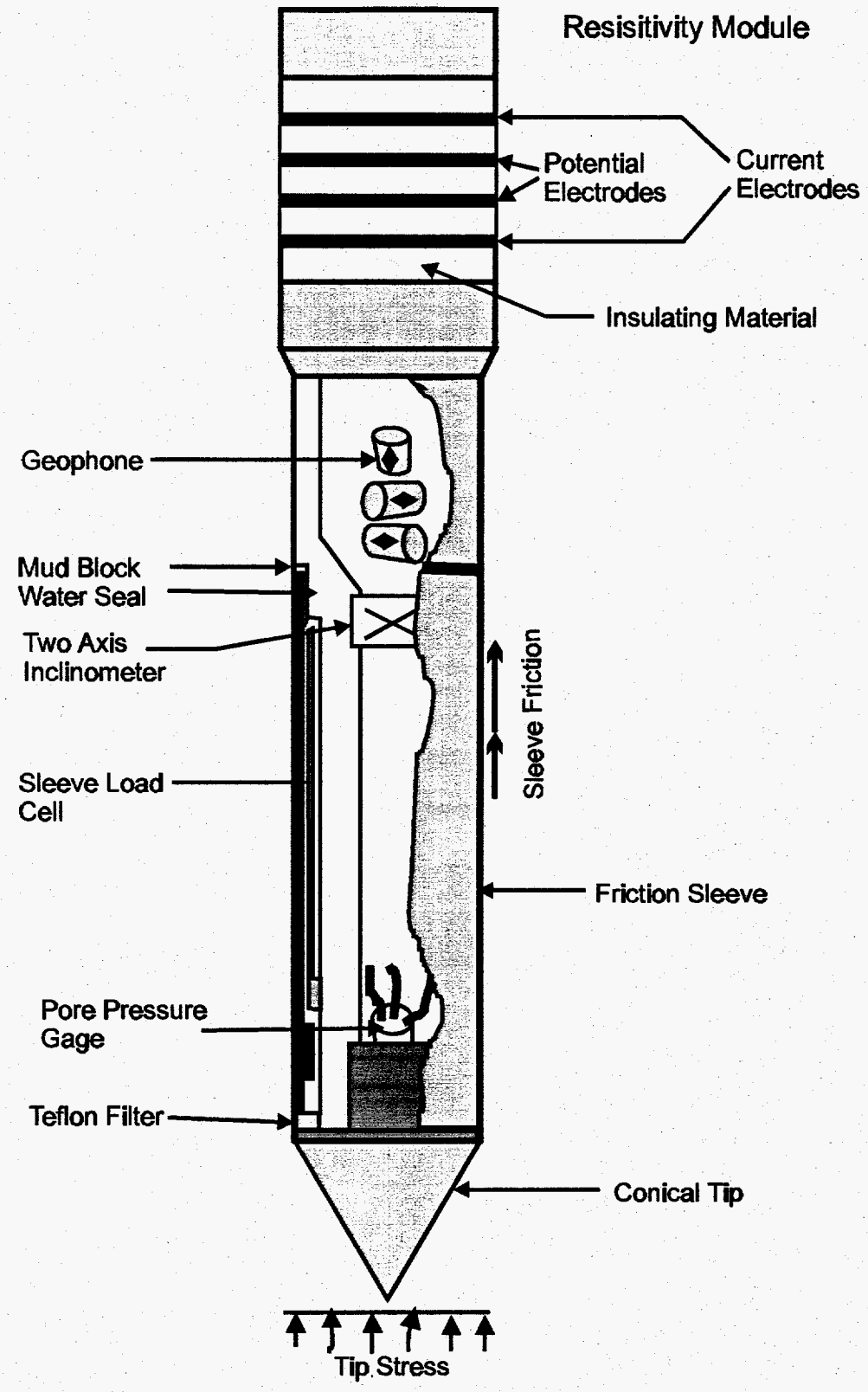

Figure 1. Schematic of ARA's cone penetrometer probe.

inches (3.658 cm or 4.445 cm). The most common for standard work is the 1.44-inch probe.

Recent environmental work, however, has led to the requirement to push deeper than possible with the 20 ton configuration. This has been accomplished by increasing the reaction weight to 30-35 tons (27,000 -32,000 kgs) and using the larger 1.75-inch probe and rod. This increases the rod buckling resistance at the higher loads. The maximum depth of penetration possible varies greatly with soil type. In soft damp soil, the 20 ton systems have penetrated 300 feet (91.5 m); but in gravely soils, such as the Department of Energy's Hanford Site in southwestern Washington, these systems met refusal at 10-20 feet (3-6 m). A thirty ton system using the larger diameter rods has reached depths of approximately 150 feet (46 m) in these same gravely soils [7].

Using the cone penetrometer for environmental site characterization represents a new application of the technology. Significant advantages of the CPT include: eliminating drilling wastes and the need for treatment and disposal of drill spoils as hazardous material; providing continuous data on the subsurface stratigraphy in real time; identifying thin layers of significantly different hydraulic conductivity; eliminating the possibility of the crew being exposed to the potentially hazardous material; reducing the possibility of cross contamination (by grouting the hole as the probe is withdrawn), and faster results when compared to conventional drilling and sampling.

In addition to being an excellent platform for making continuous measurements of contaminant information with depth, the CPT is also useful for pushing monitoring sensors into the subsurface and for taking gas, water, or soil samples for environmental testing.

1. CPT Hardware

ARA Inc. designs and manufactures CPT equipment for its own use and sale to others. Since 1982, they have pushed a combined total of over 100,000 feet and record depths of nearly 300 feet. Push depth is a function of reaction weight (e.g. the push

weight of the truck), the resistance or friction of the soil, and any impenetrable obstruction (i.e. a large boulder).

Figure 2 shows a CPT truck in operation. Four-point leveling hydraulics lift the truck off the ground and provide a horizontal platform for insuring vertical penetration into the ground. The operator stands next to the hydraulic CPT push system. Figure 3 illustrates the major components of the CPT hydraulic push system. Twin main hydraulic cylinders can apply 150,000 pounds of force. This is enough force to lift the CPT truck off the ground, hence the limiting factors become the weight or effective mass of the truck and the strength of the CPT rods. Numerous hydraulic, mechanical, and electronic safety devices have been incorporated into the basic design of the CPT push system which meet or exceed industry standards.

Figure 4 shows a larger, less mobile, skid rig which has a reaction mass of over 50 tons and can push larger rods deeper. The rig is specifically designed to be placed over single shell tanks at Hanford Washington.

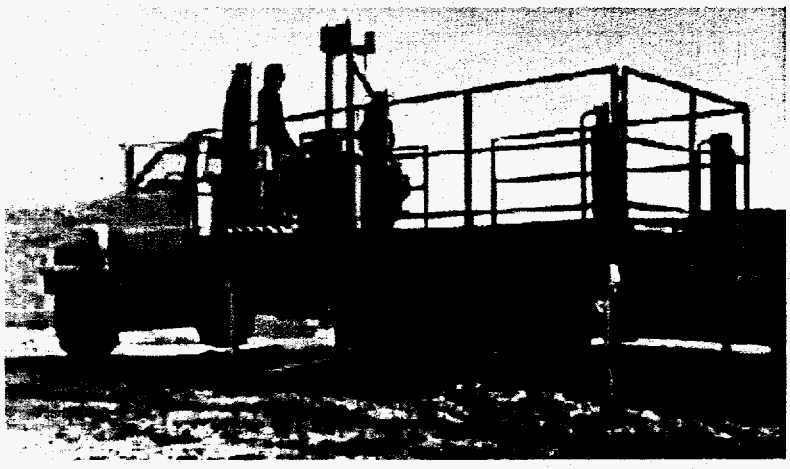

Figure 2. Open frame CPT truck.

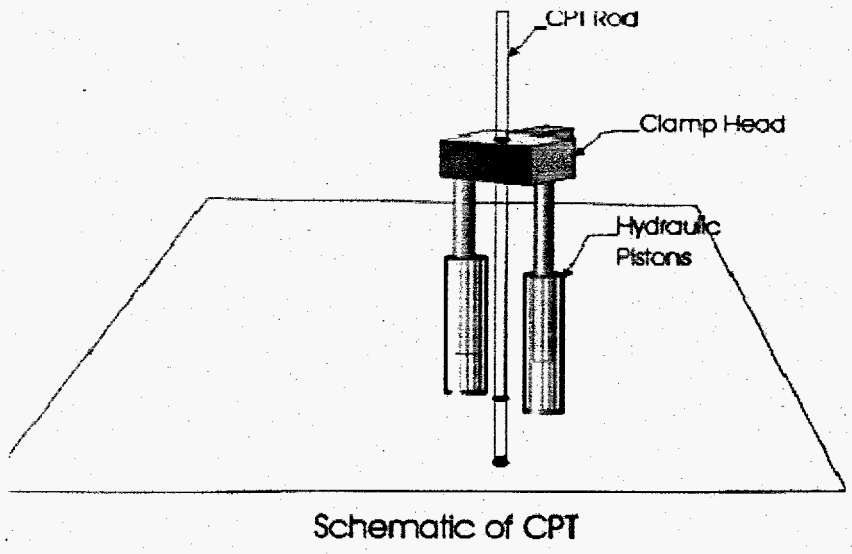

Figure 3. CPT hydraulic push system.

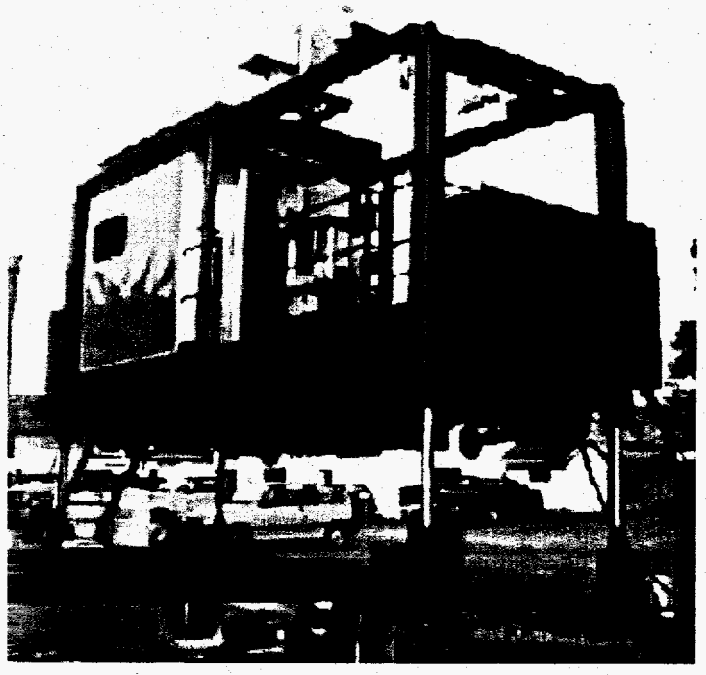

Figure 4. Hanford skid rig.

B. ELECTRICAL RESISTIVITY TOMOGRAPHY

1. Background

In most environmental restoration applications the role of electrical resistivity is to assist in characterizing a site. The task includes not only specifying the location of contamination, but also mapping the physical and chemical properties of the ground that control their distribution and movement. In the most general sense, mapping electrical resistivity is important for conditioning or constraining the hydrological models of contaminant transport and retention. These models are usually based on drill-hole tests and suffer from the problem of extrapolation of point measurements, made also between holes, to the volume between the holes.

For example, a channel of high permeability sand that is missed by a drill pattern illustrates the problem of relying solely on drill holes. This channel would be the dominant feature of the site in terms of contaminant transport. Mapping the subsurface distribution of electrical resistivity could reveal the subsurface geometry and drastically change the hydrologic model.

Soil and rock resistivity (or conductivity) measurements have been used in the mining industry for many years, and recently have been used to locate contamination plumes. The electrical resistivity of most soils and rocks depends on the conduction paths afforded by fluids in the pore spaces. Resistivity is determined by the porosity, saturation, pore fluid salinity, and clay content. Because resistivity is influenced by the dissolved solids in groundwater, mapping it may be the only direct detection method for high concentrations of contaminants that form ionic species.

ARA includes a Resistivity Module in its cone penetrometer instrumentation for measuring resistivity in the adjacent soil. As part of the CPT push rod, the module consists of four circular electrodes in contact with the soil. The electrodes are separated by insulators. The outer two electrodes are used to induce an electrical current into the soil matrix. The inner two electrodes are used to measure the strength of the induced

electric field. The amount of voltage potential drop in the electric field is a function of the resistivity of the soil.

Daily et al. [8] and *Ramirez et al.* [9] at the Lawrence Livermore National Laboratory developed and tested the Electrical Resistivity Tomography (ERT) method for mapping subsurface conditions between boreholes. Applications included monitoring water movement in the vadose zone and monitoring an underground steam injection process for soil decontamination. ERT uses a dipole-dipole measurement technique, similar to those used in conventional surface resistivity surveys [10], to measure the bulk electrical resistivity distribution in the soil mass between two boreholes. ARA is working with Dr. Daily to incorporate his research into a CPT ERT system.

Processes such as steam injection can be monitored by taking measurements before the process is started and then repeating the measurements over time as the process proceeds. Each tomographic data set is then subtracted from the original background measurements to produce a "time lapse" image set of resistivity variations between the boreholes.

2. ERT Technical Approach

To image the resistivity distribution between two boreholes, several electrodes are placed in each hole, as shown in Figure 5. This particular configuration of borehole electrodes is called a Vertical Electrode Array (VEA). Each electrode must be in contact with the formation. Two electrodes are driven by a known current, I, and the resulting voltage difference, V, is measured between other electrode pairs. This process is repeated until all the linearly independent combinations are measured. Each voltage-to-current ratio is a transfer resistance. The goal is to calculate the distribution of resistivity in the vicinity of the boreholes given the measured transfer resistance.

The ERT image creation process involves solving both the forward and inverse problems. Dr. William Daily of the Lawrence Livermore National Lab has developed and tested the computer algorithms to transform ERT data sets into tomographic images [8].

The image reconstruction plane is modeled by a finite element mesh, N elements wide (between the boreholes) and M elements long (along the boreholes). The mesh and the location of the boreholes and electrodes are show in Figure 6. Image resolution is a complicated function of many factors, including reconstruction pixel size, data signal-to-noise ratio, electrode and borehole separation, the subsurface resistivity distribution, and the degree to which the resistivity matches the two-dimensional model of the forward calculations. Resolution can be no better than one pixel; typical pixel size is 1 to 3 meters. The best resolution is obtained close to the electrodes, and the worst resolution is obtained along a vertical stripe midway between the boreholes. Thus, resolution improves as borehole spacing decreases.

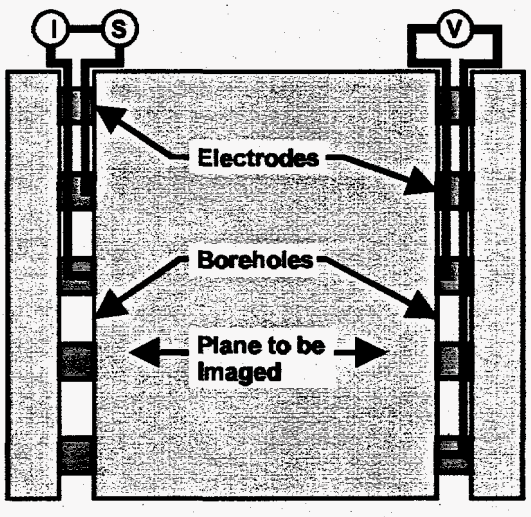

Figure 5. Schematic diagram showing data collection approach for ERT measurements.

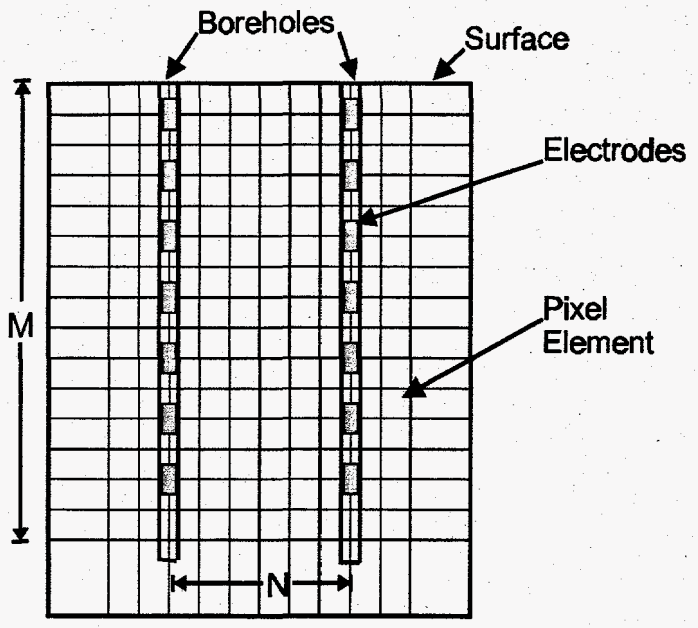

Figure 6. The reconstruction plane modeled by a finite element mesh. The pixel elements are the blocks for which electrical resistivity is calculated.

ERT relies on computer processing to form an image from thousands of data points gathered at a site. A technique called mathematical inversion is used to construct an image (tomogram) of subsurface features which have distinct differences in resistance from their surroundings. The scientist creating the tomogram generates a theoretical mathematical model. The object imaged represents what must be present to produce the actual resistance measurement data. This process is illustrated in Figure 7.

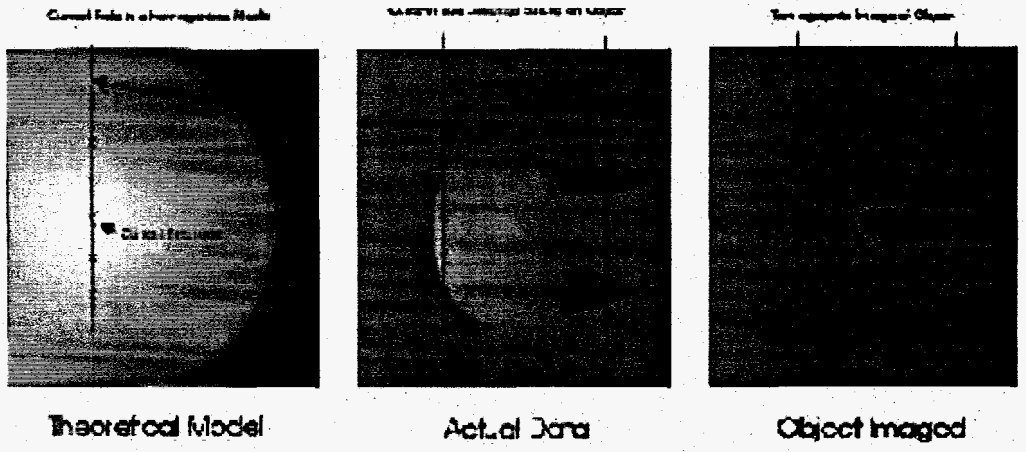

Figure 7. The drawings illustrate the process of tomographic imaging.

C. GROUND PENETRATING RADAR TOMOGRAPHY

1. Background

Ground penetrating radar (GPR) has been used for over twenty years [11-13] at chemical and nuclear waste disposal sites [14] as a non-invasive technique for site characterization [15, 16]. Standard GPR surveys are conducted from the surface of the ground providing geotechnical information from the surface to depths of 5 to 50 feet, depending on GPR frequency of operation and soil conductivity. Commercially available GPR systems operate over the frequency range 50 MHz to 1000 MHz. The lower frequencies provide better penetration but poor resolution, while the higher frequencies give poor penetration but good resolution. There are many critical environmental monitoring situations where surface GPR does not provide the depth of penetration or necessary resolution.

Borehole radar [17-19] can place the sensor closer to the region of interest, overcoming high signal attenuation in the near-surface soils. However, borehole exploration is invasive, slow and expensive because of the extensive drilling required. The radar logging tool is expensive and if not properly designed and tested will give poor results. Drilling and casing the hole disturbs the soil around the hole [20], while the air-gap between the antenna and hole strongly influences signal coupling into the formation [21]. Cable noise and attenuation in some borehole radar designs require putting electronics and power downhole [17], increasing the cost. The logging cable will distort the radiation pattern putting into question any tomographic analysis [18]. To overcome logging cable problems, fiber-optic logging cable and a downhole transmitter, receiver and battery-pack are used, greatly increasing the complexity and cost of the downhole tool.

CPT probes can acquire geotechnical data in soils in less time and at lower cost. For hazardous waste site exploration and quantifying unexploded ordinance (UXO), cone penetrometers are considered minimally invasive, since they do not bring any cuttings to the surface and can be equipped to grout the hole while withdrawing.

As described earlier, existing CPT probes measure soil and groundwater properties, such as resistivity and temperature, in the immediate vicinity of the probe. In order to extend the range around the CPT hole, ARA is developing a borehole GPR system for use in CPT installed wells.

Figure 8 is a schematic diagram showing possible data collection approaches for GPR measurements. These transmission measurements include hole-to-hole and hole-to-surface measurements. At each downhole position the surface antenna is scanned radially from the hole. For cross-hole tomography (GPRT), one CPT antenna is held stationary while the other unit is moved. The process is repeated until the volume between the holes is covered.

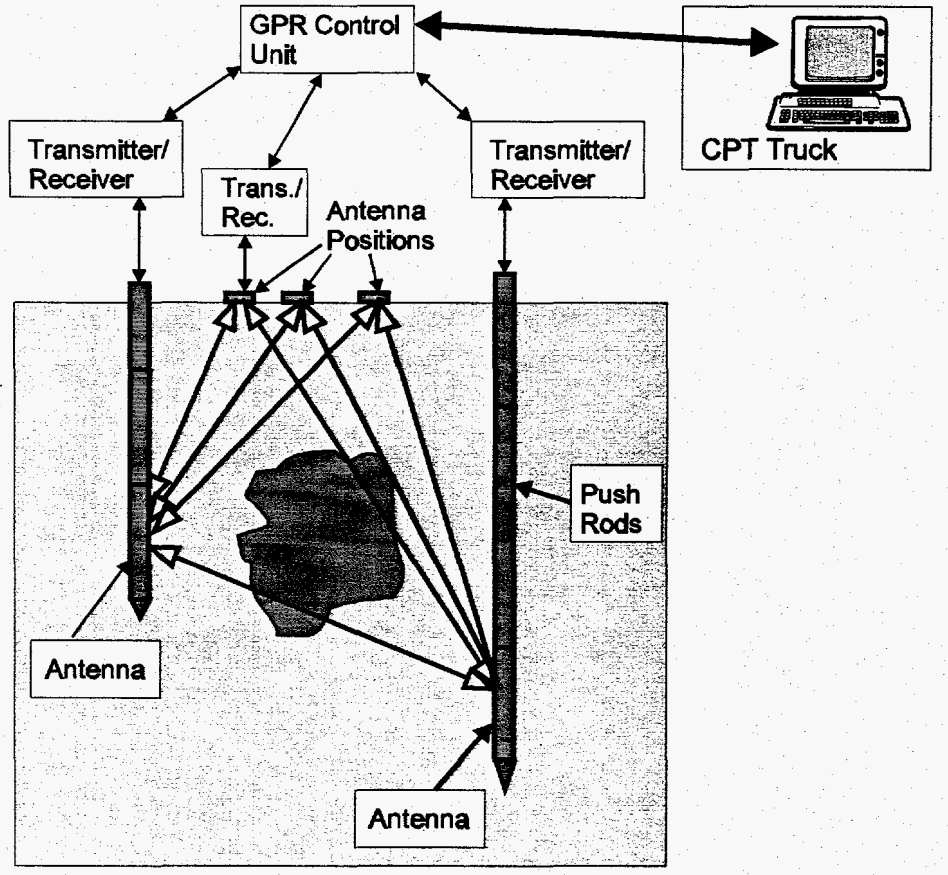

Figure 8. Schematic diagram showing data collection approach for GPRT measurements. Several ray paths are shown for typical transmitter-receiver positions on the surface and in the holes.

The interpretation of cross-hole radar data parallels the approaches used in cross-hole seismic studies. However, cross-hole data from GPR is less complicated than seismic data because the radar wavelet propagates as a single mode rather than the multitude of mode conversions that occur with seismic methods. As the radar pulse propagates, it is attenuated due to conductivity and slowed due to the dielectric constant. Therefore, GPR tomography maps variations in conductivity and velocity from which it is possible to estimate soil characteristics, such as water content, density and contamination.

For GPRT data, a tomographic reconstruction is attempted using first arrival times in an SIRT (simultaneous iteration reconstruction tomography) algorithm, initially with straight ray paths. However, if difficulty is experienced with convergence, then a perturbation method is used which allows for curved ray paths. (In the near-surface zone, the air/soil boundary may have a significant effect on shallow tomographic reconstruction and must be taken into consideration.) The region under investigation is divided into a regular grid (similar to ERT, see Figure 6), and the radar wavelet velocity and attenuation are iteratively calculated for each cell and combined to generate a color map of the region between the holes. Spatial resolution is governed by the dominant wavelength of the pulses in the medium; at 100 MHz resolution is on the order of 0.5 to 1.5 meters.

2. GPR Technical Approach

The performance of ground penetrating radar is estimated from the following set of equations. Maximum radar range is a function of radar system parameters, target parameters, and the electromagnetic properties of the materials being probed. Soil conditions govern the attenuation and velocity of the radar signal. The radar range equation appropriate for GPR is:

$$Q = 10\log[\frac{P_{\min}}{P_t}] = 10\log(\frac{E_t E_r G_t G_r v_m^2 g e^{-4\alpha R}\sigma}{64\pi^3 f^2 R^4})$$

where Q is the system performance factor in decibels (dB) and the various components are:

System dependent:

P_{min}	=	minimum detectable power
P_t	=	transmitter output power to antenna
E_t and E_r	=	antenna efficiency
G_t and G	=	antenna gain
f	=	frequency of operation

Media dependent:

v_m	=	velocity of propagation in medium
α	=	attenuation coefficient of medium

Target dependent:

g	=	back scatter gain of target
σ	=	target scattering cross-section area

Range Dependent:

R	=	distance to target from antenna.

Commercially available GPR systems advertise Q values from about -100 dB to -150 dB, the lower value is without computer processing while the larger value (-150) is with processing. Antenna efficiency and antenna gain are influenced by the type of soil and the coupling of the antenna to the soil. Part of this project was to optimize the antenna design in relation to the medium it is immersed in for maximum gain and efficiency. The operating frequency is a design parameter that was investigated for various operational and deployment configurations.

Velocity of propagation in the soil is a function of the soil mixture dielectric constant [11,13] and is primarily governed by water content. Radar signal attenuation is controlled by soil conductivity. Clay soils are conductive, thus radar range is limited to a few feet. Sandy soils are much less conductive and penetration depths are on the order of 100 feet. Dielectric mixture theories [24] are used to calculate the complex dielectric constant of four-phase soil mixtures for modeling the radar propagation response and

interpreting measurement results. Mixing models take into account soil density (solid particle and air volume), water volume, and contaminant volume.

Figure 9 is a plot of maximum radar range as a function of frequency for three different target types -- a smooth plane reflector, a rough plane reflector, and a point scatterer. As frequency of operation decreases the maximum range increases for plane reflectors, such as boundaries between soil and bedrock or dry and wet soil. For point targets, such as boulders or metal drums, maximum range increases with frequency because the target radar cross-section is larger at the higher frequencies. However, at even higher frequencies the target is no longer a point scatterer and its response approaches a plane reflector.

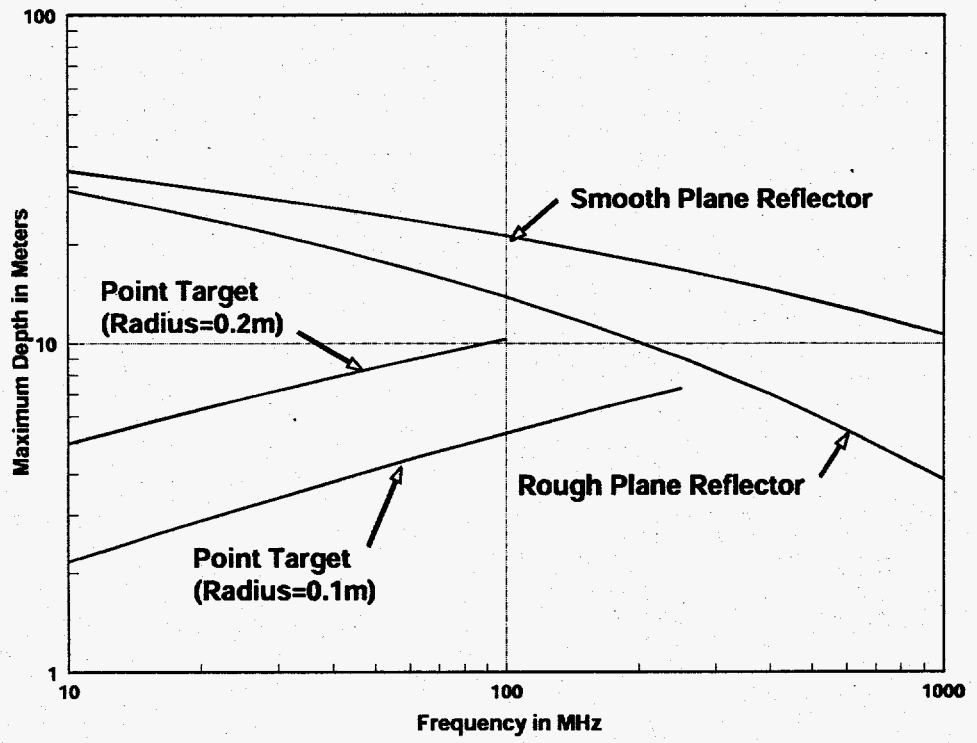

Figure 9. Maximum radar range for three target types. (Q = -110 dB, dielectric constant = 6, and conductivity = 0.001 S/m.)

Figure 10 shows the influence of soil conductivity on maximum radar range at three frequencies for a rough plane reflector. Note that low conductivity sands are much

more transparent than clays. Water content is not as important as the conductivity of the water. Penetration depth is roughly the same for moist and saturated sand as long as the conductivity is the same.

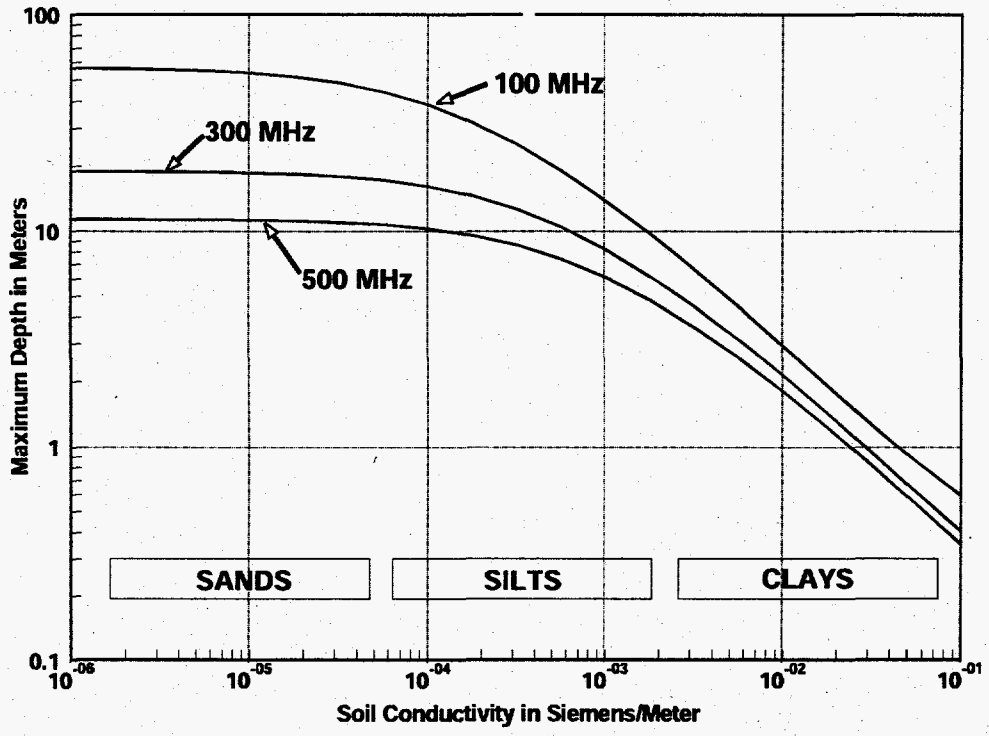

Figure 10. Radar range to a rough plane reflector, such as bedrock. The soil types are general designations. (Q = -110 dB and dielectric constant = 6.)

D. SOIL MOISTURE SENSOR

A Soil Moisture Sensor (SMS) was used during the field evaluation tests of the ERT and GPR systems. The Soil Moisture Sensor logs the moisture content of the soil surrounding a borehole as the probe is advanced down the hole. Since radar propagation in soils is strongly influenced by moisture content, SMS measurements help with GPR interpretation.

There are several field methods by which the soil moisture content can be monitored. These include neutron logging, suction lysimeters, gypsum blocks which relate

the resistivity of the gypsum block to water content, electrical resistivity of the soil and relating the soil dielectric constant to soil moisture content. Neutron logging devices are expensive and may not function properly at sites with radioactive contamination. Lysimeters, gypsum blocks, and soil electrical resistivity methods all require detailed calibration which is expensive and time consuming since the calibrations must be made for each soil of interest.

The dielectric properties of a soil are closely related to the soil moisture content. Soils, in general, are composed of air, solid particles, and water. In the frequency range from 10 to 1000 MHz, the dielectric constant of the dry particles is about 4, air is 1, and water is 80. Therefore, the measurement of the dielectric constant of soil mixtures offers a sensitive measure of soil moisture

The ARA CPT soil moisture sensor uses a Resonant Frequency Modulation (RFM) approach to determine the dielectric constant and, ultimately, soil moisture. This approach consists of installing a custom designed circuit board in a CPT probe which is then interfaced with standard CPT equipment, eliminating the need for specialized measurement equipment. A second advantage of this approach is that cable distances are unlimited as all conditioning and processing of the signal occurs downhole, eliminating the effect of cable length induced signal attenuation.

The RFM approach uses the probe and surrounding soil to set the resonant frequency of an oscillator. The RFM circuit frequency used in ARA's soil moisture sensor varies from 100 MHz in air to approximately 75 MHz in tap water. The basic principal of the probe is that a portion of the soil between two rings in contact with the soil will form part of a electronic circuit which has a frequency of:

$$f(t) = \frac{1}{2\pi\sqrt{LC}} \qquad (2)$$

where: L = inductance

C = capacitance, and

L is a fixed constant

The capacitance has two components that set its value: 1) a fixed parameter of the probe, "C_k."; and 2) a value that changes with the surrounding soil moisture, C_v. The combination of C_K and C_v will change by ≈ 30 pf from air to water with ARA's probe.

The final equation relating the frequency of oscillation of the circuit to the capacitance of the soil is:

$$f(t) = \frac{1}{2\pi\sqrt{L(C_K + C_v)}} \tag{3}$$

As 100 MHz signals are difficult to transmit without using coaxial cable, signal conditioning is done downhole which reduces hardware and cabling problems. The RFM signal is counted downhole and outputs a TTL clock signal in the range of 20 kHz. The TTL clock frequency is then converted to an analog signal. This conversion was made in order to condition the signal into a 0-4 volt output, which is compatible with a standard CPT or other data acquisition.

1. Soil Moisture Sensor Design

The sensor unit of the SMS is made from two stainless steel rings about 1-1/2 inches in diameter and between 0.25 and 1.0 inch long, encapsulated on a plastic housing as shown in Figure 11. The diameter and length are a function of the specific application and desired "region of influence". The rings form a capacitor which is part of the feedback loop of a high-frequency oscillator operating at about 100 MHz. The oscillator and other electronic components are mounted on the PC board. As the dielectric constant of the material near the rings changes, the frequency of the oscillator shifts. The frequency shift range is converted to a 0-to-5 volt signal. The sensor readout is connected by a long cable to the in-hole sensor. Calibration correlates frequency shift, and therefore voltage readout, with known moisture content.

Location of the PC board in relation to the electrodes is critical to the stability and repeatability of the SMS. At 100 MHz, the SMS is like a small radio transmitter/receiver and is very susceptible to radiated feedback from distributed conductive systems.

Transmission line characteristics between the oscillator and electrodes must be controlled. Therefore, the electrodes and electronics are calibrated as a unit.

The expected frequency shift from dry soil to saturated soil (0.5 moisture volume fraction) is on the order of 25 MHz. Thus a frequency span of 25 MHz represents a span of 0.5 moisture volume fraction in soil moisture, depending to some extent on soil type. Therefore, the expected resolution of the SMS is on the order of ±0.025% moisture volume fraction. Since the response is nonlinear the sensitivity will be greater at low moisture content.

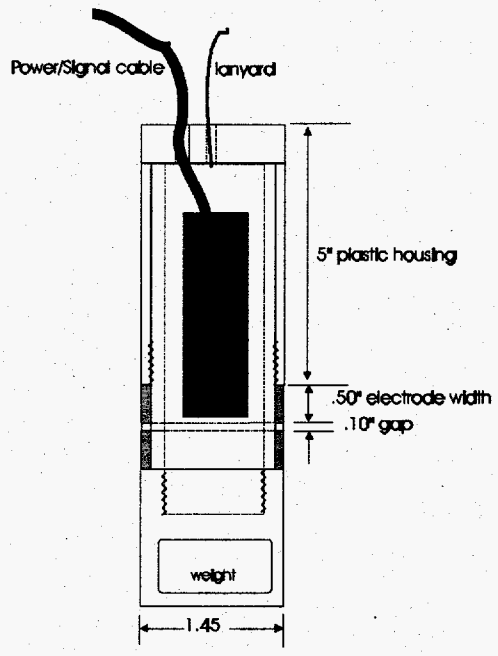

Figure 11. Soil Moisture Sensor for use in PVC access tubes.

2. SMS Calibration Cell

ARA has built a calibration cell for laboratory soil moisture measurements and for calibrating the soil moisture sensor. Figure 12 is a photograph of the calibration cell which is composed of a clear plastic cylinder 12 inches in diameter and 60 inches long with 1 inch diameter holes spaced along the length of the plastic cylinder. These plugged holes are used for extracting soil samples during an experiment for determining the soil moisture

by gravimetric methods. A 2 inch diameter PVC access pipe is positioned along the axis of the 60-inch cylinder. The SMS prototype, Figure 13, is moved through the access tube.

A known quantity of sand fills the cell and measured amounts of tap water are introduced into the soil column at the bottom of the plastic cylinder. (The weight of the calibration cell is constantly recorded.) Note in Figure 12 the plastic plumbing on the left side of the cell; this also allows determination of the artificial water table level. After the system has stabilized an SMS profile is measured. As an example in Figure 12, the water table is at 23 inches from the cell bottom (37 inches from the top), while the water-staining of the sand is visible at about 33 inches; thus there is about a 10 inch capillary fringe.

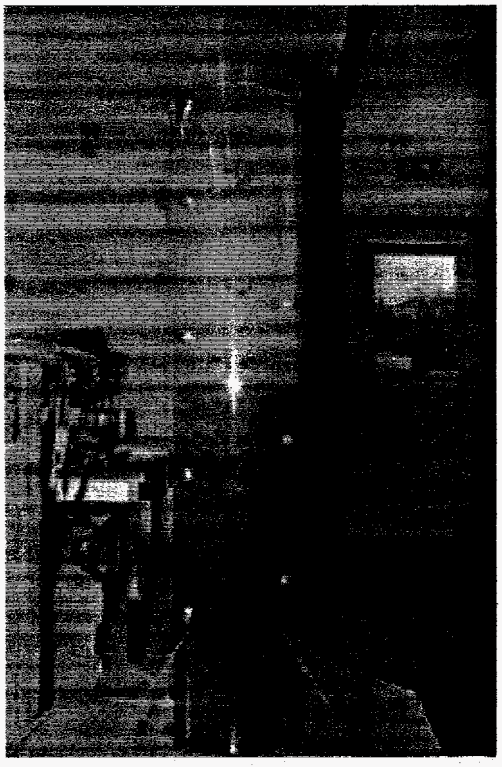

Figure 12. SMS calibration cell.

Figure 13. SMS entering access tube.

After the SMS measurements, small soil samples are removed with a 1-inch diameter metal tube, as shown in Figure 14, at appropriate locations along the cell. The volume, weight and moisture content of the samples are determined and used to calibrate the SMS readings. Two soil samples are taken at each depth and the results averaged.

Figure 14. Sampling tube in preparation for extracting a sample

Figure 15 is an example of an SMS profile in the calibration cell. The horizontal scale is the soil moisture content by volume in percent. Volumetric moisture content is derived from the measured SMS voltage and the soil sample calibration data. In the example, dry sand extends from 0.5 to 2 feet. The soil moisture increases through the capillary fringe from 2 feet to 3.2 feet to the saturated condition, demonstrating the sensitivity of the SMS bore hole probe.

In the fully saturated region volumetric moisture content represents the soil porosity and thus is a measure of soil density. Note in Figure 15 that the saturated soil moisture content decreases below 4 feet from 38% to 34%, indicating that the soil density is greater at the bottom of the cell.

Prior to deploying the SMS in the PVC monitoring wells, the SMS probe is placed in two sample volumes of known moisture content, dry and saturated, representative of the end points of the probe voltage. The sample volumes are dry and saturated sand of

measured volumetric water content. These two voltages must correspond to the cell calibration values.

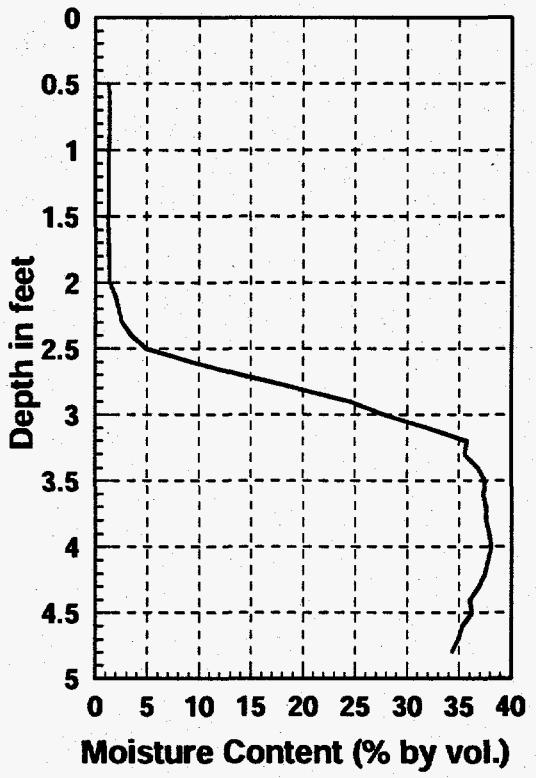

Figure 15. Example of SMS data from the calibration cell with dry sand to a depth of 2 feet and saturated sand from 3.2 feet to the bottom of the cell.

SECTION IV.
HARDWARE DEVELOPMENT

A. ERT SYSTEM DEVELOPMENT

ERT system development consisted of three primary tasks:

1. Vertical Electrode Array (VEA) design for CPT installation.
2. ERT electronics hardware.
3. Software for control and imaging.

1. VEA Design

CPT is routinely used by ARA to rapidly install plastic, PVC-lined monitoring wells. The PVC pipe is placed on the outside of the push rod and is attached to the push rod only at the bottom. This allows the PVC to be pulled down into the hole to eliminate compressive forces and minimize breakage. However, this installation process stresses the threaded joint between PVC pipe sections, limiting the installation method to relatively low friction soils, e.g. sands and clays. (Since the GPR borehole system requires a plastic lined hole for the antenna, this CPT method is used for the VEA.)

PVC well installation follows a two stage procedure. First a "dummy" hole is formed using 1.75-inch diameter rods, and the rods are then extracted, leaving an open hole. The crew switches to 1.4-inch CPT rods. Threaded sections of PVC are then slid over each section of rod and the central rod is are pushed down the pilot hole pulling the PVC casing with it. The inner push rods are extracted leaving the outer PVC well casing, or a VEA.

The VEA design consists of installing alternating sections of PVC tubing and stainless steel electrodes. Figure 16 shows the components for this design: the 1-1/2 inch PVC (2 inch OD) pipe, the stainless steel electrode element and the wired-spring

contacting assembly. This contactor is installed after the PVC-SS VEA has been pushed into the ground and the CPT truck clears the site. Sections of ½-inch-diameter PVC pipe, alternating with each spring contactor, are threaded, bead-like, onto a central cable. The entire assembly is put together on site as it is being inserted down the VEA "well". The drawing in Figure 17 illustrates the final installation.

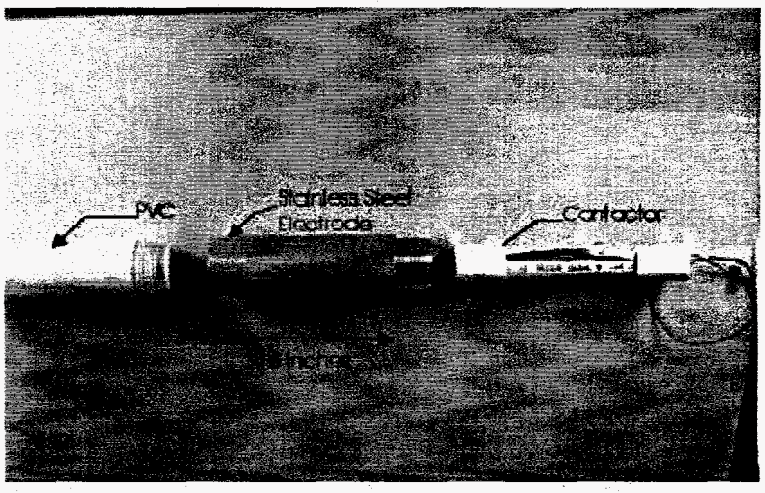

Figure 16. PVC and stainless steel electrode assembly.

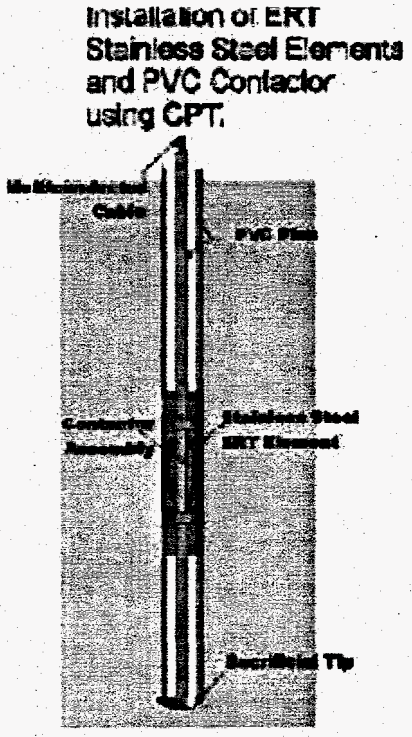

Figure 17. PVC-SS electrode VEA illustration.

Initial field testing indicated that the contactor assembly was too fragile and too difficult to remove without breaking the ½-inch-PVC pipe. Also, the spring contactor surface in contact with the inside of the SS ERT element was limited to essentially a two-point contact. A second, interim solution was to use the existing stainless steel fingers on the signal cable without the ½-inch PVC pipe. While this design did work and imaging data taken successfully, other issues such as ruggedness over repeated deployments, strain on the multi-conductor cable, storage problems, and low electrode contact area made this design less desirable.

A second contactor assembly was designed, built and tested. The preliminary design shown in Figure 18 was drawn up and a prototype built out of aluminum. The machining for this design was felt to be excessive, so a cost reduction analysis was made and the final design shown in Figure 19 was selected.

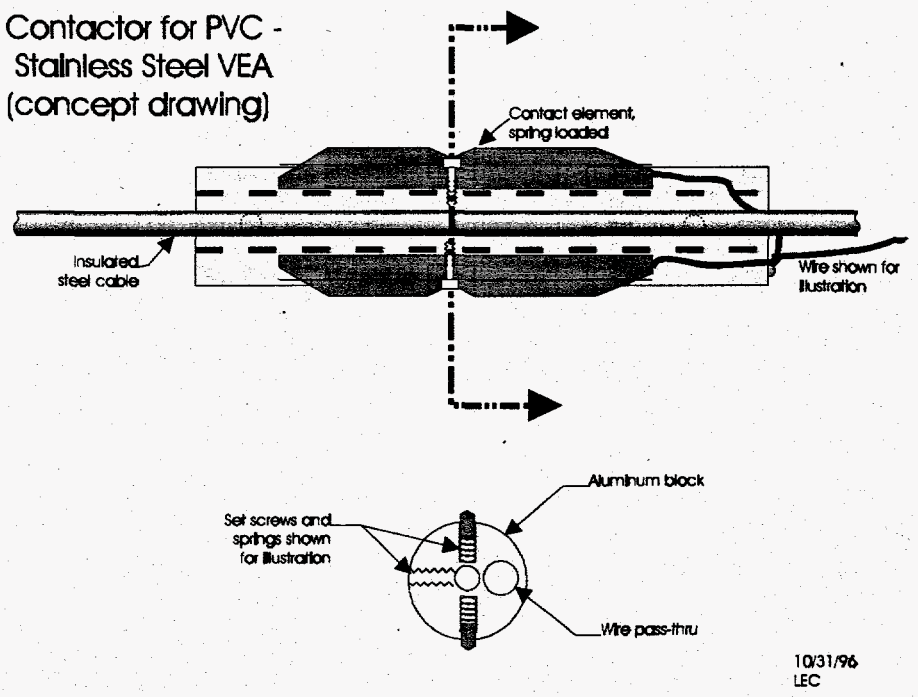

Figure 18. Preliminary ERT contactor design.

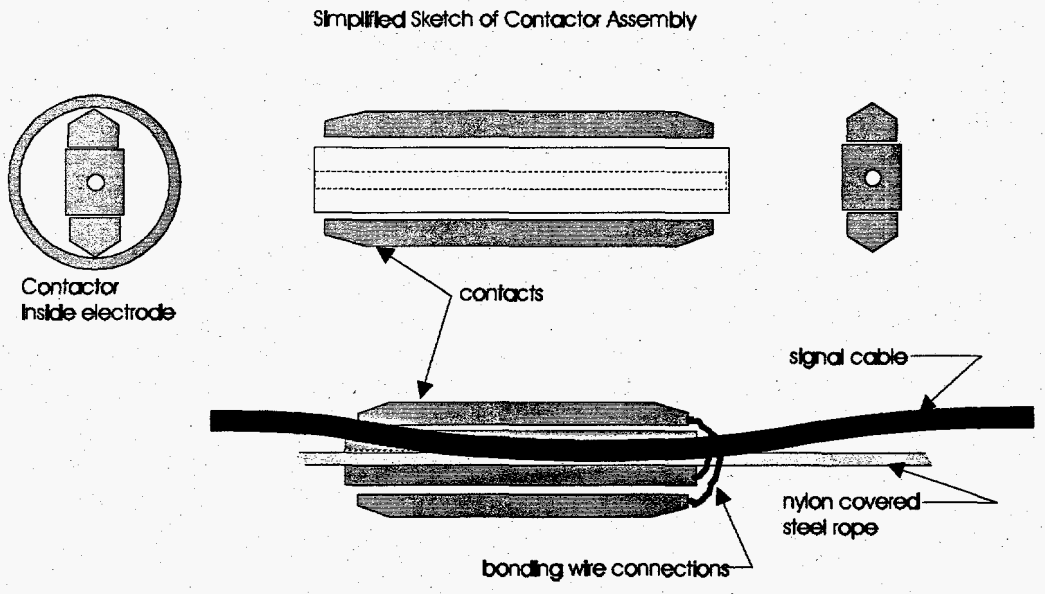

Figure 19. Final ERT contactor design.

The two contact units are spring loaded to the central cable housing, thus forcing the contactors against the inside of the electrode. A prototype was built and springs were sized using a friction pull scale. Contact resistance tests were made with a VEA mockup and the contactor performed well. Forty contactors (for four VEA's with 10 electrodes each) were built and firmly attached to the nylon covered steel rope at intervals corresponding to VEA electrode spacing. Each contactor was then connected to the appropriate wire in the cable bundle for electrical connection to the ERT electronics. A weight was attached to the lower end of the steel rope to counter the contactor friction as the final assembly was lowered into the VEA.

Figure 20 is a picture of the contactor assembly being lowered into a GeoWell. (The term GeoWell is used for the CPT installed PVC/SS-electrode well that was also used for the GPR cross-hole measurements. In other words, a GeoWell is a well in which multiple sensors can be deployed.) No significant problems were encountered as the contactors were deployed into the GeoWells. The contactor arrays are easily removed, wound up on wire reels, and stored when not in use. They are easily redeployed and relocated back in the GeoWells and indexed to the proper electrode location in a matter of minutes. Figure 21 is a schematic of contactors deployed in a GeoWell.

Figure 20. ERT contactor entering GeoWell.

Figure 21. ERT contactors in GeoWell.

There are several important advantages to this CPT installation method of VEA GeoWells:

- The electrodes are in *intimate* contact with the soil formation by virtue of being pushed into the soil; whereas, in a borehole environment, they need to be grouted in place and fluid sometimes injected to minimize contact resistance.

- Installation *costs* are substantially reduced over that of borehole techniques, thus allowing more measurement holes using CPT. With more holes surrounding the soil volume, the resultant tomographic images are clearer and less ambiguous.

- Standard PVC well installation procedures can be used with no need to grout the hole.

- A hollow well is left in the ground for other possible uses, such as GPR tomography and the soil moisture sensor.

- Long-term robust installation.

Disadvantages include:

- Inability to perform installation in difficult gravely soils, i.e. Hanford, WA.

- Electrical connection to the SS electrode using spring contactor requires a clean hole.

- Two CPT pushes are required per VEA installation.

2. Electrode Testing

Various tests are routinely performed on VEAs once they have been installed and prior to data acquisition to test various aspects of an ERT network. Some of these tests are checks that wiring and installation have been performed properly while other tests estimate data quality. Some tests are between electrodes within a vertical array -- termed intra-array tests -- while others are performed between two or more VEAs -- termed inter-array tests.

An intra-array test (loosely termed the "pole-to-pole" test) which checks the wiring to each electrode was conducted on each VEA. This test identifies problems such as: 1) the wiring to two electrodes being inadvertently reversed, and 2) wire insulation being accidentally scraped during installation, thereby creating a current injection or potential measurement point in a location not intended. The test also checks the contact impedance between each electrode and the surrounding soil to assure that sufficient electrical energy is imparted to the ground. Results of these tests demonstrated that the electrodes and wiring for each VEA were functioning properly.

To detect spurious signals from sources such as nearby electric lines, the wave forms of received signals from the VEA electrodes were inspected using an oscilloscope. Although spikes of an unknown origin were observed, there was no 60 Hz interference as might be expected from buried electrical lines or overhead power lines.

The degree to which electrical data can be successfully inverted by tomographic methods to produce an accurate image of the subsurface resistivity structure depends largely upon our knowledge of data quality. Several tests are frequently performed to determine the quality of ERT data. These are checks on the electrode environment and the subsurface resistivity structure, not the data acquisition electronics. For example, these tests determine the degree of electrical coupling between the electrode and the surrounding soil. They also help to determine the stability of the subsurface resistivity environment during the time of data acquisition These tests are as follows:

- Repeatability
- Reciprocity
- Superposition
- Linearity

Although none of these tests quantitatively define the measurement error, an estimate of that error is given. There is no way to directly detect measurement error *in*

situ without apriori knowledge of the subsurface resistivity structure. Therefore, the strategy is to devise schemes, using the above tests, to estimate error with as few measurements as possible.

Repeatability involves taking the same measurement many times without changing the measurement system. When repeatability is used as a noise estimator, it is conducted as an inter-VEA test. The experience with repeatability has been as follows:

- It is an easy method to use and can generate substantial information in a relatively short time.
- It is difficult to guarantee that the subsurface resistivity structure is not changing. It is best therefore, to repeat the measurements as close in time as possible when the subsurface can be expected to be nearly static.
- Repeated use of transmitting electrodes within a short period of time can under some conditions, electrically polarize them as a result of electrochemical reactions at the metal-electrolyte interface. This polarization degrades the measurement in a way that does not happen normally, yielding a biased error estimate.
- Under other conditions, when electrode polarization is small the method produces a low estimate of the true error.

Because repeatability can easily give a biased or low noise estimate, it is seldom used to estimate measurement error.

Another test that may be conducted as either an intra- or inter- VEA test is reciprocity. This test consists of repeating the measurement but with the transmitter and receiver dipoles interchanged. In an ideal linear system, i.e. when Ohm's law holds, each measurement and its reciprocal will yield identical results. Perfect reciprocity of this kind is a fundamental assumption enabling the measurements to be inverted for the resistivity structure. Experience with reciprocity tests shows that:

- Although not as easy to perform as repeatability, it can generate statistical information on errors in a reasonable time period.

- Between the time the normal and reciprocal measurements are made, it is necessary to assume that the subsurface resistivity structure is static.

- The method is sensitive to polarization of the transmitting electrodes as explained in the discussion on repeatability.

From experience, reciprocity has been found to be the best estimate of measurement error for ERT data. Due to its importance, the normal and reciprocal measurements are automatically collected as a standard part of the acquisition measurement schedules.

Another test that checks the data quality is based on the principle of superposition. Superposition must be satisfied for any linear system. For a given transmitter dipole, potentials on three electrodes *a*, *b*, and *c* will be such that

$$f_{ac} = f_{ab} + f_{bc}$$

where *f* is the potential drop between two electrodes. This states that the potential differences measured between electrode *a* and electrode *c* must equal the sum of the potential differences measured between electrodes *a* and *b* and electrodes *b* and *c*. The degree to which this equality is not true is an estimate of data error.

The experience with error analysis from superposition measurements is as follows:

- It is difficult to use because it required at least three measurements and several calculations to get a single error estimate. Also it is not easily configured in the acquisition measurements schedules.

- As with the other methods of error estimates, it is assumed that the subsurface resistivity structure is static during the time of the measurement

Experience has shown that the error estimates obtained from applying the method of superposition are similar to reciprocity estimates. It is used primarily when a problem is found to involve a few known electrodes. This fact combined with the application difficulties results in low usage of the law of superposition for error analysis.

As mentioned above, superposition tests the ERT system, including the subsurface, for linearity. For a system to be linear, the potential drop measured on a particular receiver dipole must be linearly related to the amount of current being transmitted on another particular dipole. To check for linearity, the transmitting current must be changed as consecutive measurements are made for each dipole pair. Consequently checks for linearity are made only when other test methods indicate that it is required.

3. ERT Electronics Hardware

Several commercial manufacturers of resistivity measurement equipment were evaluated. Apparently, none of these systems are specifically suited to cross hole applications. All of the vendors offer equipment which works well with surface electrodes. One manufacturer, Zonge, has recently added a multiplexer to their product line which specifically addresses cross hole measurements, yet Zonge did not have one of these products readily available.

Table 1. ERT Data Acquisition Hardware Comparison Chart

	IRIS	OYO	Zonge A	Zonge B	U of AZ	Keithley
Cost ($)	11K	50K	56k	85K	25K	22K
Channels	1	32	4	30	30*	50
Cost/Channel?	11K	1.5k	14K	2.7K	0.78k	0.5K
Size/Weight	10 lbs	40 lbs	100 lbs	100 lbs	200 lbs	40 lbs
Automatic/Manual	Manual	Auto	Manual	Auto	Auto	Auto
Battery Portable?	Yes	Yes	Yes	Yes	No	No
Upgradable/Expandable?	No	No	Yes	Yes	Yes	Yes

	IRIS	OYO	Zonge A	Zonge B	U of AZ	Keithley
Flexibility for Research (1-10)	1	3	8	8	10	10
Tech Support?	Yes	Yes	Yes	Yes	No	No
Field Repairable?	No	No	No	No	Yes	Some
All the above data acquisition systems would require a computer workstation to generate tomograms. (~$5k)						

a) Manufacturer Commentary:

IRIS: SYSCAL JUNIOR, a single purpose field portable instrument for measuring resistivity. This is a single channel instrument (combines transmitter and receiver) which can be used in conjunction with an "intelligent electrode nodes system", it's usefulness is limited to a small number of electrodes. A limited data set can be downloaded into a laptop PC. Our experience with this instrument, was measuring resistivity with two VEAs at the Vermont Test Site. Four hours was required to take each data set from ten pairs of electrodes. An external battery set is required. An external computer and relay multiplexer system would be required to automate resistivity measurements. Control software would have to be written.

OYO: McOHM-21, a single purpose portable instrument for measuring, processing and displaying resistivity (combines transmitter and receiver). A built in CPU and hard disk make this unit truly self contained though the programming for borehole ERT is limited. Data processing for tomograms still requires an external computer. The cost noted above includes a 32 channel scanner (multiplexer) such that two VEAs of 16 electrodes can be addressed. A number of scanners can be daisy chained together and it is possible to access a total of 750 electrodes. A 12 volt rechargeable battery is included.

Zonge A: GDP-32 electrical methods receiver, ZT30 Transmitter, and ISO/1 in combination is a multifunctional, multipurpose electrical geophysical instrument with which ERT data can be gathered. A built-in CPU controls the instrumentation. Data must be downloaded into a laptop or PC for storage and

analysis. The configuration above is for four channels and assumes a necessary breakout box to access large ERT arrays. This unit is extremely rugged and field ready and represents the state of the art. A 12 volt rechargeable battery is included.

Zonge B: GDP-32 electrical methods receiver, ZT30 Transmitter, and ISO/1 and MX30 multiplexer (scanner) in combination is a multifunctional, multipurpose electrical geophysical instrument with which ERT data can be gathered. An external laptop or PC is required in the field control these units for large ERT arrays. Data must be downloaded into a workstation or PC for storage and analysis. This configuration has 30 channels and allows access to two, 15 electrode VEAs. This unit is extremely rugged and field ready and represents the state of the art. A 12 volt rechargeable battery is included. This configuration has been purchased by Lawrence Livermore National Laboratory for their ERT research.

U of AZ: (University of Arizona, Dr. Douglas LaBrecque) This planned instrument would utilize a Hewlett Packard power source as the transmitter and HP voltmeters as the receiver. Combined with signal conditioning and signal multiplexing of UAZ design, this rather large, rack mounted instrument would be extremely flexible as a research instrument, though not particularly adept in field conditions. A PC or laptop would be required to control this instrument though the data storage and processing could be included for the possibility of real-time tomography. Thirty multiplexed (*) channels were assumed for cost estimating. Increasing the channel count for this system, which is still under development, would be relatively easy and additional cost would be minimal. A 120 volt external power is necessary.

Keithley: This multipurpose source/measure system designed for the semiconductor test industry is extremely cost effective though not proven that it would work in the ERT application. Coupled with a 100 MHz PC, this system would be extremely fast at taking data. External AC power is required.

It was decided to use a multiplexer and a source/measurement system from the commercial test equipment industry. Hewlett Packard, Tektronics and Keithley equipment were reviewed. The Keithley equipment has the best overall value and some of it could be

rented. Therefore, a Keithley Model 238 source/measure instrument was rented. Purchasing the multiplexer, a Keithley 7002 with 8 each 4X5 relay matrix cards, was necessary since no matrix equipment could be found in the rental market. TestPoint ™ general purpose test instrumentation software was purchased to run the equipment via the GPIB (IEEE-488 Bus).

The Keithley equipment performed well using dummy loads in the laboratory. However, in the field, the wide dynamic range of currents required to excite the electrodes (500 microamps to 100 milliamps) made data gathering very difficult. A second Model 238 was ordered and integrated into the system such that a constant voltage could be applied to the electrodes and the induced voltage measured from the other Model 238. After much effort it was discovered that the noise levels were unacceptable. Failing to find a technical solution, it was decided to use an Iris Syscal Junior connected to a computer for automatic data acquisition and the Keithley multiplexer to switch between electrodes.

A Syscal Junior was rented and integrated into the system. Still reciprocity noise levels were found to be unacceptable. It was discovered that the battery powered Syscal Junior, linked to the computer via the RS232 port, had a ground connection which eventually found it's way to the power grid and earth ground. So, in effect, we were always looking at an extra electrode in the array which seriously affected the noise level and would invalidate any possible imaging data. This noise problem was eliminated after the AC power ground line was lifted from the computer.

4. Hardware System Design

Manufacturers of resistivity measuring hardware have not designed their equipment for borehole, cross hole configurations. The essential ingredient in such a system is a flexible relay matrix with a high channel count. Commercial field portable hardware does not exist in the market today. Perhaps the reason is that subsurface resistivity measurements require higher amounts of power to produce the required high current densities. The Syscal Junior at 50 watts power would be the minimum transmitter

required. Zonge, for instance offers a 1000 watt unit. At these power levels, the relays for the matrix would have to be quite large, heavy and expensive. An interim and flexible solution is to use a commercially available relay matrix system which could be reconfigured upon demand for the number of VEAs at the site and the total number of electrodes.

The 4 X 5 matrix card in Figure 22 has four inputs and five outputs and in this case, allows the four signal lines from the Syscal Junior to be multiplexed to any of five electrodes. Two cards are required for each VEA of ten electrodes, and eight cards total for the four VEAs used in the Vermont field tests. With eight 4 X 5 matrix cards, each electrode in the array of 40 electrodes can be connected to any of the four Syscal Junior signal lines, as partially depicted in Figure 23.

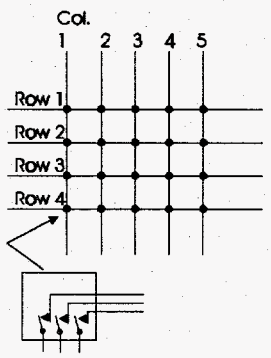

Single Keithley 7052 4X5 matrix card
200VDC, 500ma carry, 10VA max

Figure 22. Schematic of the 4 X 5 matrix card.

The matrix cards are housed in a chassis which furnishes relay actuation power and control logic. The chassis (Keithley 7002) accepts inputs manually, or in this case over the GPI Buss. The 7002 has a 500 location local memory. A sequence of relay patterns can be loaded into each location and saved even after power is shut off.

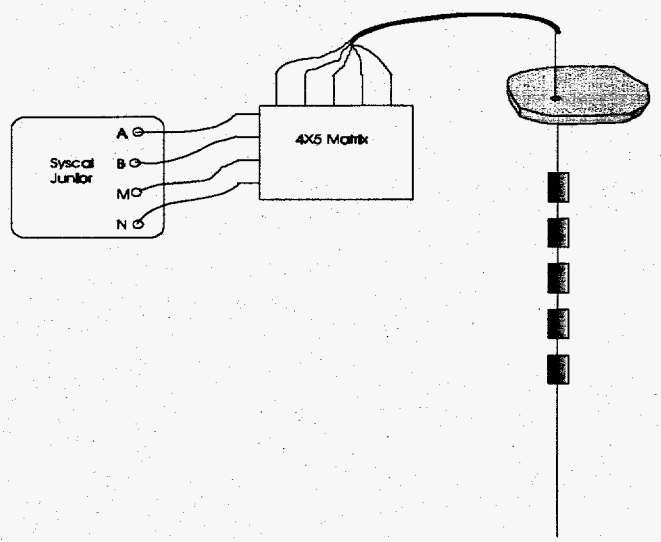

Figure 23 Partial system schematic.

Figure 24 shows a PC, running Windows and the TestPoint application software, controlling the Keithley 7002 relay matrix over the GPIB The PC asynchronously starts the IRIS Syscal Junior and then receives ERT data over the RS232 port. Though clearly not an optimized system, it works well enough to allow one measurement to be taken every 30 seconds.

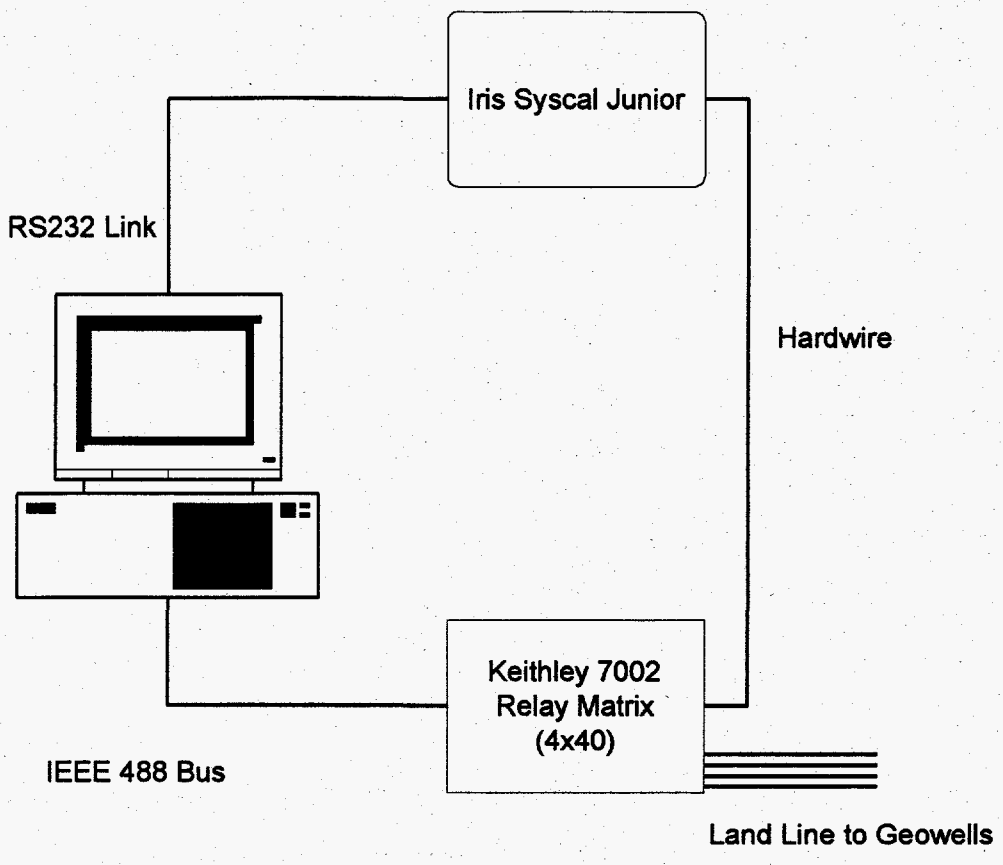

Figure 24. ERT system diagram.

Figure 25 is a software/hardware flow diagram. An Array Schedule File is set up depending upon the ERT measurements to be made. Generally all possible independent combinations of electrode pairs are measured. The total number of independent measurements is equal to $\frac{n(n-3)}{2}$, where n is the number of electrodes. Thus, for two VEAs with 10 electrodes each, n=20 and the total number of independent ERT measurements is 170. The reciprocal of each independent measurement is also made in order to quantify the noise level for the forward inversion and imaging program. Therefore, the Array Schedule File will contain a sequence of 340 measurements in our example. For this example and the equipment used, the total measurement time for one borehole-to-borehole ERT measurement is about 3 hours.

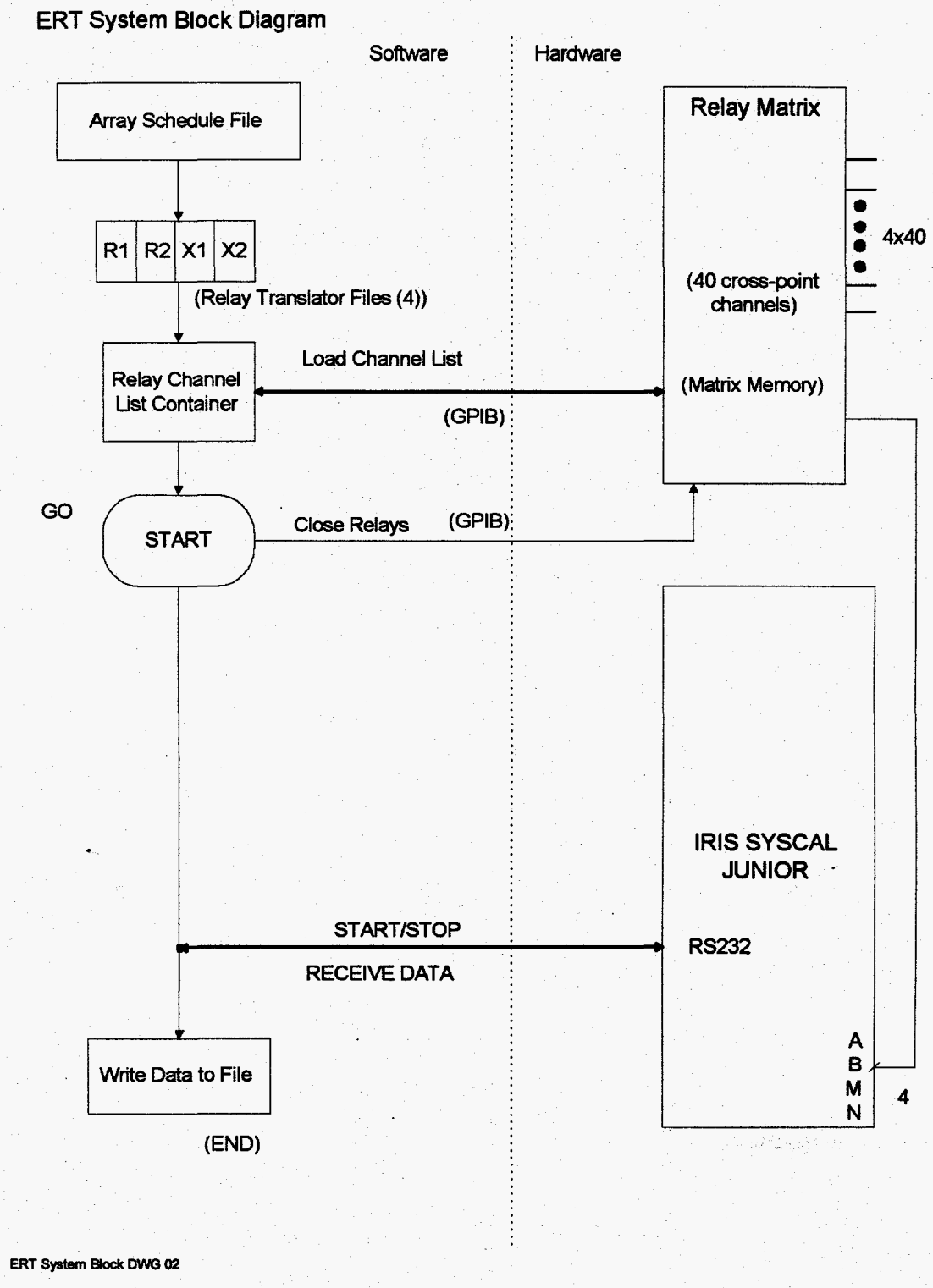

Figure 25. ERT software/hardware flow diagram.

5. Software

The software used for processing the ERT data was supplied by Abe Ramirez and Bill Daily of Lawrence Livermore National Laboratory. The underlying algorithms are described in [25-26]. Here we summarize some of the key features.

The inversion process involves iteration between sets of forward and inverse calculations, with changes of parameters in-between. The goal of this process is to make the final forward calculation match the field data to a certain specified degree of accuracy. The code solves for the resistivity structure in a half space based on electrical resistivity measurements taken between discrete electrodes residing in two or more co-planar boreholes. The code is loosely referred to as 2.5D, which means that the earth resistivity structure is assumed to be two dimensional (i.e. resistivity varies only in the plane defined by the boreholes), yet the problem is solved at some level in three dimensions to allow for the fact that the electrodes used for injecting and receiving measurement signals are discrete points in 3-D space. This mixture of 2-D and 3-D philosophies is implemented via a Fourier transform technique. This improvement over a pure 2-D method allows the electric field around the electrodes to be modeled properly, yet avoids the difficulties and time constraints of solving a pure 3-D problem. The boundary conditions used in this method are (1) no current flow out of the ground at the earth/air interface (Neumann condition) and (2) a constant zero potential at the other three subsurface mesh boundaries (Dirichlet condition). The three subsurface mesh boundaries are set at a large distance from the measurement boreholes.

The general problem of tomographic inversion of electric potential data for the resistivity structure from boreholes in the earth is both ill-posed and non-unique. This problem stems partly from the fact that full surrounding coverage of the region of interest is not possible. Therefore, some additional constraints referred to as "regularization" must be placed on the solution for the inversion to converge. In this implementation of the problem, the most desirable solution is one that (a) gives a minimal difference between the forward calculation and the measurements, and (b) has the smoothest spatial variability in the resistivity structure consistent with (a). This additional constraint is sufficient to allow

the inversion to converge to a stable and repeatable result. The method requires that an estimate be made apriori of the variance of each measurement, that is the variability or scatter to be expected if many repeated identical measurements were to be made. This variance is necessary to calculate a weight or degree of confidence in the particular measurement, so that one or more noisy measurement values will not unduly affect the results. Actually estimating the variance of each measurement by repetition is impractical due to time constraints, but experience has shown that the difference between each measurement and its reciprocal is the most useful estimate of this parameter.

B. GPR HARDWARE DEVELOPMENT

GPR borehole system development consists of three primary tasks:

1. Antenna design for CPT installation.
2. GPR electronics hardware.
3. Software for control and imaging.

1. Antenna Design

GPR systems require antennas that can radiate temporally short, wide-bandwidth pulses in the 50 MHz to 1000 MHz frequency range. Therefore, the antenna should have the following characteristics:

- The radiated pulse should be a faithful reproduction of the transmitter output.
- There should be little pulse distortion and ringing on the radiated pulse.
- The reflected signal at the input to the antenna should be small, on the order of 30 dB or more below the input pulse.
- The amplitude of the radiated pulse should be as large as possible.

An infinitely long biconical dipole is the ideal radiator for short, ultra-wideband pulses, meeting all the above criteria. Resistively loading a finite length biconical dipole provides the most practical antenna design for pulse radiation [27]. The resistive loading is meant to eliminate or greatly reduce the reflections from the ends of the dipole, creating a traveling-wave antenna [28]. When placed in a borehole, antenna characteristics, modified by the surrounding medium, are quite different from that in free space [29].

Several antenna design approaches were studied, including making the antenna an integral part of a CPT push rod assembly. From the electromagnetic (EM) prospective the antenna should be intimately coupled to the surrounding soil to maximize energy transfer, yet maximally decoupled from any metallic control cables and CPT push rods. Mechanical loads on the radar probe restrict the design considerations and the types and thickness of dielectric materials. Also, if the antenna is built into a CPT rod assembly, a CPT truck is required as part of the GPR data acquisition process. The truck is needed to move the antenna/push rod assembly up and down the hole.

After careful consideration it was decided to design the GPR antennas to operate independently of the CPT truck, except that CPT methods are used to install the GPR boreholes much like the ERT installations. In fact, tests were run to demonstrate that the same PVC/SS-electrode-lined holes could be used for GPR measurements – the GeoWells. Using GeoWells for both ERT and GPR is an important development which improves data fusion and reduces survey costs.

Figure 26 is a schematic of the final GPR borehole antenna design. The antenna is constructed from a 7 foot long piece of 1-inch diameter PVC pipe over which copper foil is glued to form the dipole elements. The antenna is connected to the surface with a low-loss coaxial cable. At the cable-antenna connection a ferrite balun is inserted to transform the unbalanced cable currents to the balanced dipole. A properly designed balun decouples the cable from the antenna, thus reducing distortions in the radiation pattern due to the presence of the metallic cable. The antenna assembly is covered with plastic to provide a moisture resistant protective coating. Figure 27 is a picture of the two GPR

borehole antennas and Figure 28 shows an antenna prior to deployment in a borehole. Vertical radiation pattern measurements were made in the ground indicating that the antennas are well behaved.

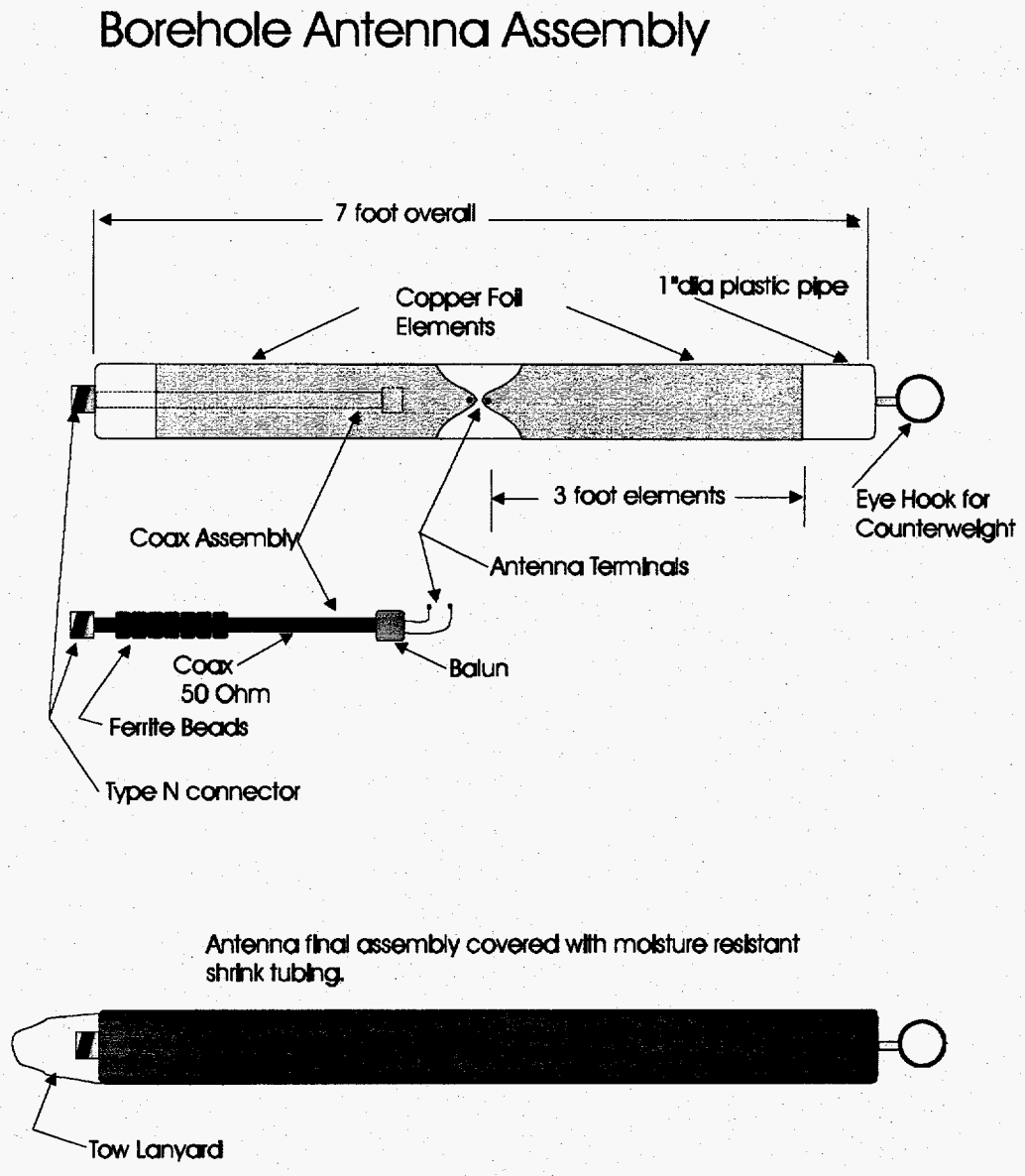

Figure 26. GPR borehole antenna schematic.

Figure 27. Picture of GPR borehole antennas.

Figure 28. GPR borehole antenna ready for deployment.

2. GPR Electronic Hardware

Several manufacturers of GPR equipment were evaluated. Apparently none of the vendors sells a borehole system suitable for our application. All the vendors offer equipment which works with surface antennas.

Table 2. GPR Equipment Comparison Chart

Manufacturer	GSSI-SIR2	Sensors &Software pulseEKKO 100A	RAMAC/GPR
Cost	**$53,350.00**	**$44,005.00**	**$33,500.00**
Control Unit	$23,000.00	$27,000.00	included
Antenna Set, 120MHz	$16,000.00	$10,000.00	included
Software*	$7,700.00	included	included
Accessories	$1,650.00	$2,005.00	$2,500.00
Computer Workstation	$5,000.00	$5,000.00	$5,000.00

*GSSI has quoted both RADAN and WINRAD-ACT software which will automatically pick datapoints and enter them into a spreadsheet.

Sensors and Software includes an integral software package which picks datapoints automatically.

RAMAC/GPR from Sweden is a complete system for taking surface GPR measurements and would require some modifications / additions to perform borehole measurements.

A GSSI SIR2 electronics system was rented and used to perform the initial testing of the borehole antennas. Figure 29 is a picture of the equipment and antennas. The antennas are partially shown in the foreground and the 100-foot down-hole cables are coiled in the background.

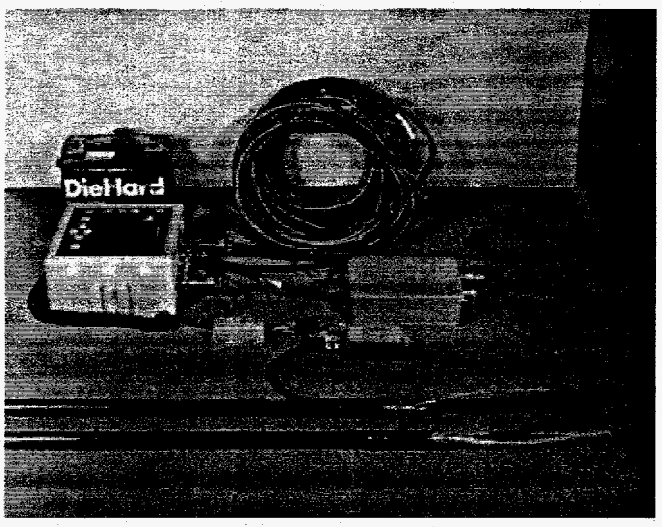

Figure 29. Picture of GPR borehole test equipment.

The GSSI system is optimized for surface measurements where the antennas are towed across the ground; this equipment was not well suited for borehole measurements. Therefore, Sensors and Software PulseEkko1000 electronics equipment was used for the GPR borehole testing program. The radar control unit was interfaced with a laptop computer as shown in Figure 30. A 100 MHz monocycle, short pulse transmitter was

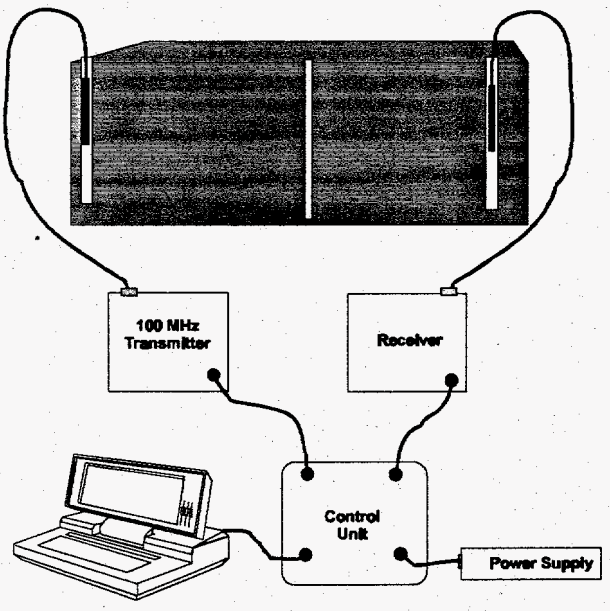

Figure 30. GPR equipment setup for tomographic measurements.

used. Transmitter parameters and data acquisition settings were set via the laptop computer (Toshiba Tecra500). Received waveforms were stored on this computer's hard drive.

3. GPR Software

Several steps are followed to assure GPR data quality for software processing. The radar data acquisition software permits the viewing of individual return wavelets in oscilloscope format in order to verify system integrity. In this viewing mode we can observe excessive noise due to hardware problems or cable distribution as well as return signal amplitude values. While data is actually collected in "wiggle trace" viewing mode, we examine the return wavelets in oscilloscope mode before actual data collection of each borehole pair and a number of times during collection. In order to improve signal-to-noise ratio, a fixed number of consecutive scans (e.g. 64) are averaged for each transmit/receive location. Each averaged scan is stored in a separate computer file and the file name and test conditions recorded.

After field data collection is finished, each data scan is preprocessed using a bandpass filter to remove high frequency noise and low frequency offsets. The power envelope of the scan is calculated and compared with the average amplitude If the maximum value of the power amplitude is less than three times the average value then the scan is removed from the data set.

The software used for processing the GPR borehole data to generate tomographic images is 3DTOM [30]. 3DTOM is a DOS compatible computer program developed by the US Bureau of Mines for three dimensional tomographic imaging of the subsurface at mine sites. The program uses the simultaneous iterative reconstruction technique (SIRT) to invert travel time data and produce maps of wave velocity, or to invert amplitude data and generate maps of wave attenuation coefficients. The SIRT algorithm employs an initial guess model. The corresponding travel times for the ray paths are then calculated and compared to the experimental data. The differences between the calculated and experimental travel times are used in calculating correction factors to be applied to the

initial model. This procedure is repeated until some convergence or limit criterion is reached. The correction factors are calculated for all path simultaneously. Either seismic or electromagnetic wave data may be used.

Ray tracing in 3DTOM uses several different methods, including ray bending, network theory, and a combination of these. User-defined constraints are important in reducing the mathematical non-uniqueness of inversions based on limited data. 3DTOM permits the use of hard constraints, or soft constraints based on fuzzy logic, to allow for uncertainty in the constraints.

SECTION V.
RESULTS AND DISCUSSION

This section presents the results of the field tests at the ARA Vermont Test Site. The discussion describes the test site, GPR surface survey results, CPT push results, ERT and GPR topographic images, and the SMS results. The results are very encouraging and show a strong correlation between all the test methods — CPT, ERT, GPR, and SMS.

A. SITE DESCRIPTION

ARA's Vermont site was chosen as the field test site because it is close to our offices and we had some previous CPT experience at this site. However, a more important consideration was that it contained inter-bedded sands and clays with variable moisture content; thus it contained at one site a range of electromagnetic subsurface conditions for testing the ERT and GPR capabilities.

The ARA Vermont Test Site is an open grassy field on a hill approximately 160 feet above the White River in South Royalton, VT. The soil is inter-bedded sands with clay lenses and thin clay layers; the water table is about 160 feet below the surface. The test plan included installing four GeoWells on a square grid with an infusion well at the center of the square. ERT and GPR tomographic data would be taken before and after the infusion of about 100 gallons of salt water.

The surface topography was measured and a GPR surface survey was performed to map the near-surface soil stratigraphy. An initial interpretation of the GPR profiles indicated that the possible flow direction of the water from the infusion test would be in the northwesterly direction. The position and orientation of the GeoWell grid was chosen from these GPR survey results. A reasonable push depth for our tests is 60 feet, which then dictated a maximum hole spacing of 30 feet for the ERT tests. (A rule of thumb is to have the well spacing ½ the depth or length of the ERT array.) The CPT truck installed the four GeoWells and the infusion well along with three additional monitoring wells. A photograph of the test site is shown in Figure 31. The heated instrumentation trailer is in

the background with the GeoWells and Monitoring Wells identified in the foreground. Figure 32 shows the dimensional layout of the test site.

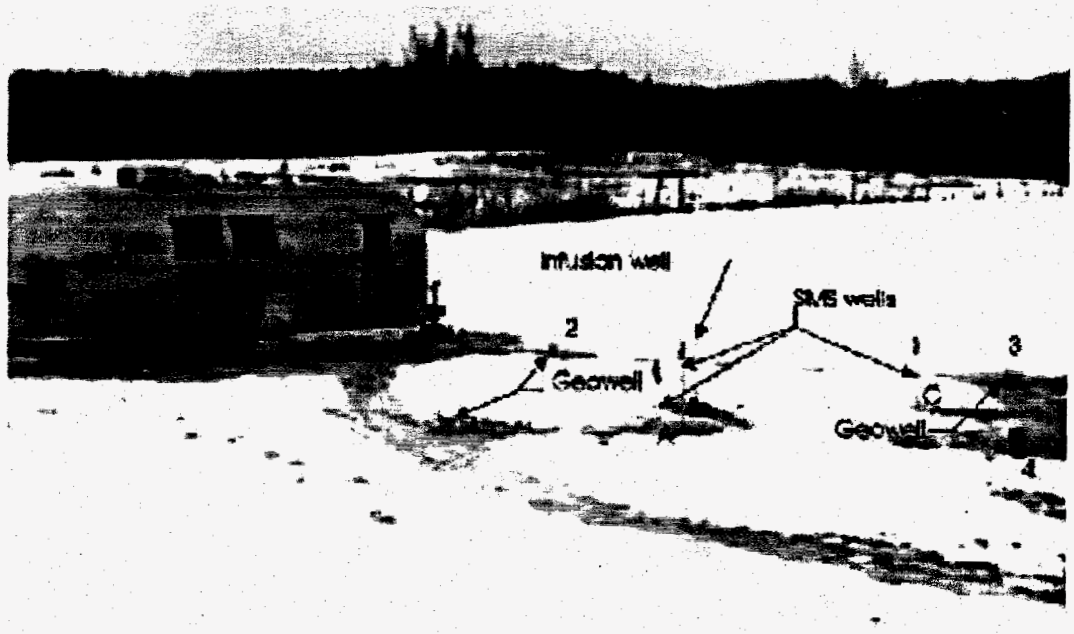

Figure 31. Picture of the Vermont Test Site.

1. GPR Surface Survey Results-

Prior to making the survey and installing GeoWells, the site was staked out and grid lines 10 feet on center were laid out over a 100 x 100 foot square centered about the well site. Theodolite data were taken and surface features plotted (see Figure 33).

A GSSI ™ GPR system with a 500 MHz antenna was used for the survey. Scans were made in both the North-South and East-West directions. Event markers at each 10 foot interval were placed in the data record by the operator during the scan. Figure 34 shows two examples of radar profiles with the GeoWell locations superimposed on the "raw" radar records. These profiles are orthogonal to each other. The prominent reflection features are thin clay layers; the blank areas are homogeneous sand.

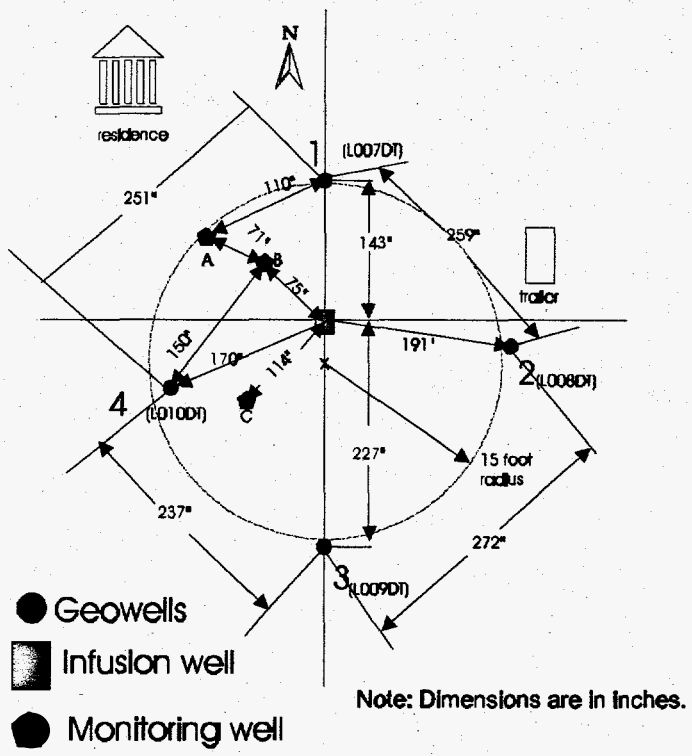

Figure 32. Layout of GeoWells at the Vermont Test Site.

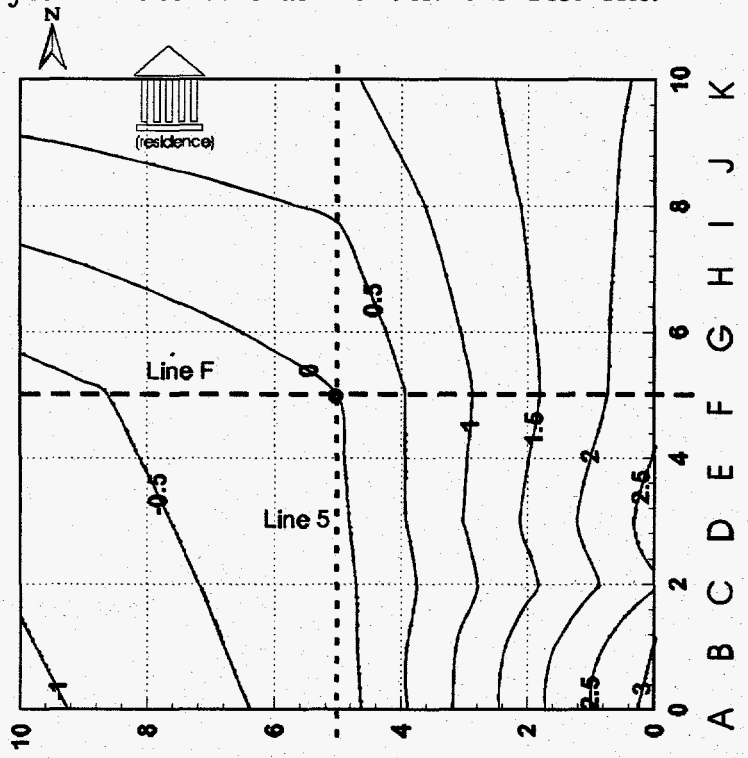

Figure 33. Surface contours in feet at Vermont Test Site.

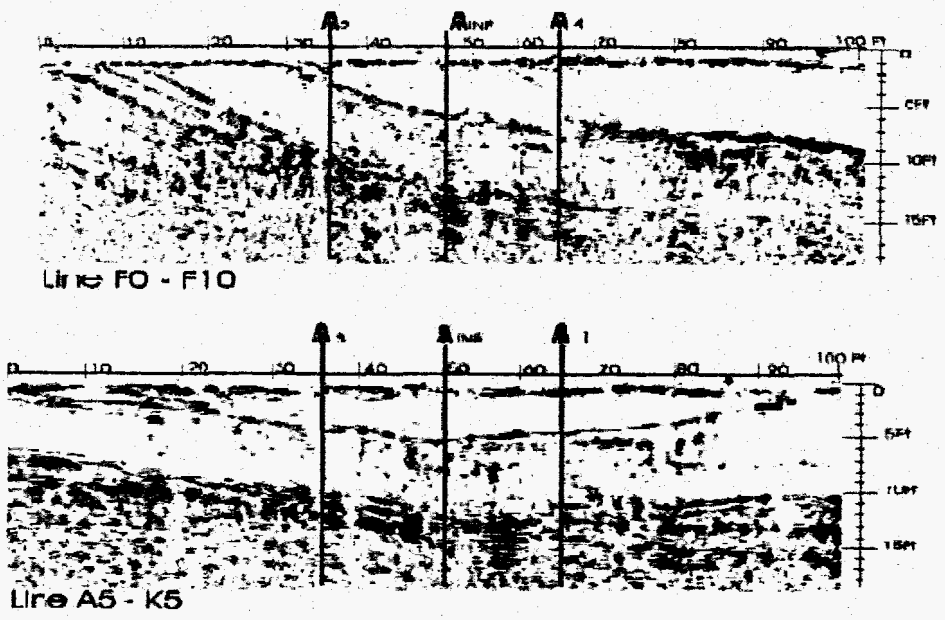

Figure 34. Examples of GPR profiles.

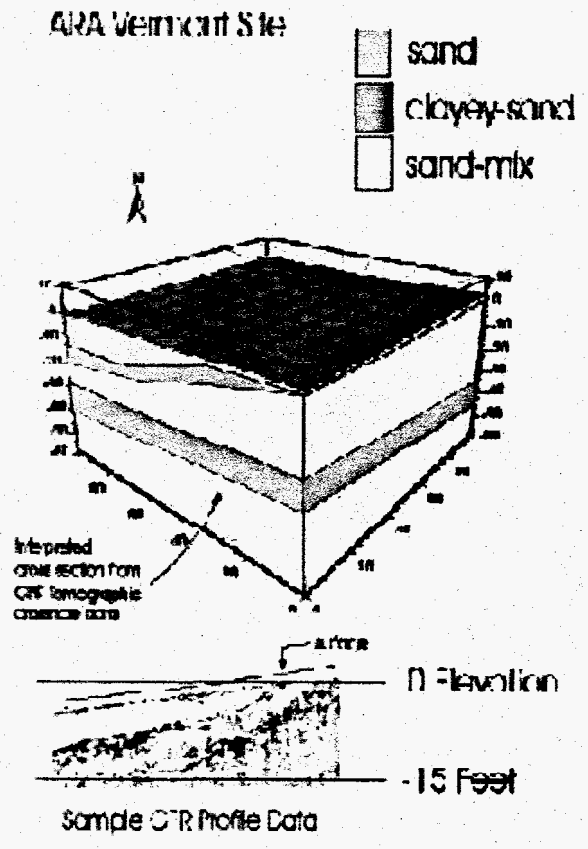

Figure 35. 3D map of major subsurface layers.

The radar profiles were interpreted to produce a 3D map of the major subsurface layers to a depth of about 20 feet as shown in Figure 35. Figure 36 is a contour map of the first major clay layer. The location of the monitoring wells and holes 1 and 4 were selected to intersect the projected direction of the salt water plume.

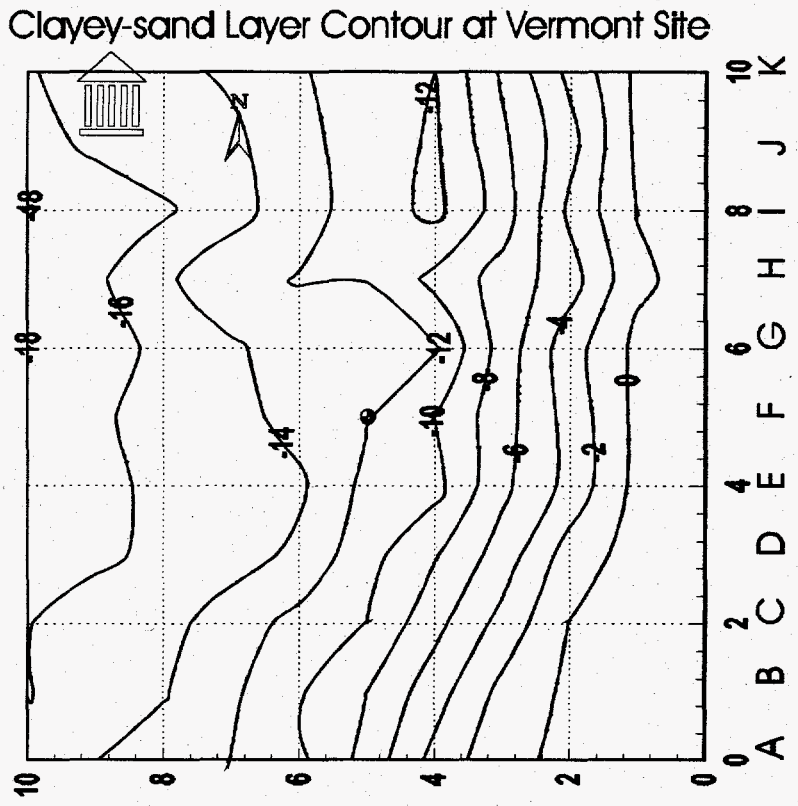

Figure 36. Contour plot of first clay layer from radar profiles.

2. CPT Results

Standard CPT pushes were made at each of the GeoWell locations prior to installing the GeoWells. CPT logs of tip, sleeve, pore pressure, and resistivity data were recorded at each well location. The CPT logs are plotted in Appendix B. Figure 37 shows the soil classifications calculated from the CPT logs using industry standard classification routines. These CPT data are eventually compared to GPR and ERT data. Note that the depths to the inter-bedded clay layers are fairly consistent from hole to hole. The pore pressure logs (Appendix B) indicate that the clay layers are very wet.

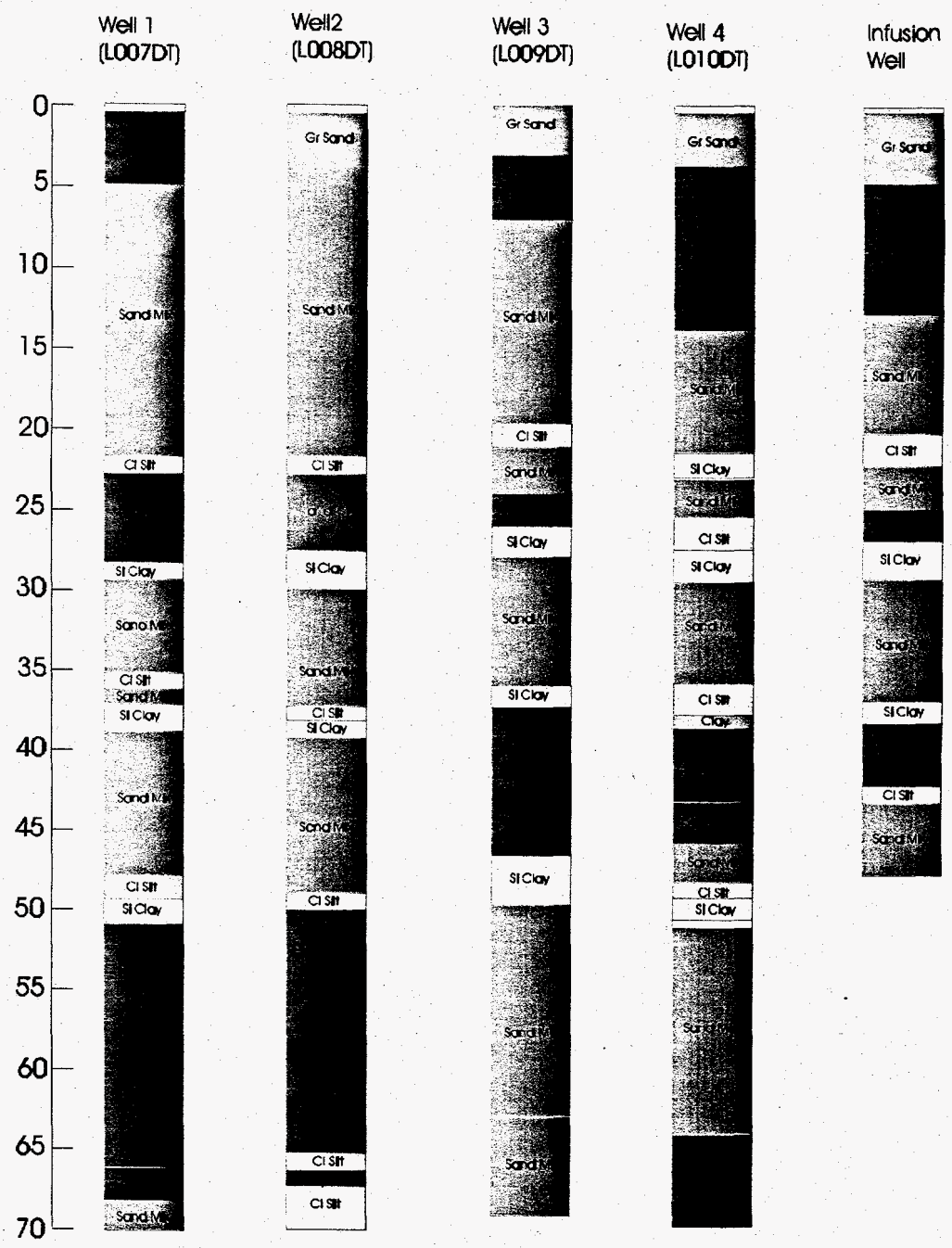

Figure 37. CPT soil classification logs at GeoWells.

Combining the surface topography plot and the GPR profiles with the CPT data, the depth to soil interfaces from a horizontal datum plane is calculated. The top of the first clay layer is at approximately 15 feet below the surface at the center of the grid. Using real-depth measurements from CPT records and contiguous records from GPR data, this clayey layer was easily located and mapped (see Figure 36). (In the CPT logs,

this boundary is between the Sand and Sand Mix classification.) This clayey layer dips towards the northwest while the surface contour dips towards the south. Based on this information, we speculated that the saline water introduced at the infiltration well should flow in the northwesterly direction.

3. GeoWell Installation

Several field trials were made to determine the most effective method of installing GeoWells. During these procedures, two types of well casing material were tried: PVC and reinforced fiberglass. The goal was to install a GeoWell in a single push versus reoccupying a well hole after a "dummy" CPT push. Four condition sets were attempted:

- Single push with standard sacrificial tip
- Single push with oversize tip
- Reoccupying with standard sacrificial tip
- Reoccupying with oversize tip

In both cases using the oversized tip, no difficulty was encountered installing the GeoWell to a desired depth (see Figure 38). For the case using the standard tip, both PVC and fiberglass separated from the tip, causing the push to be abandoned. The case of reoccupying a "dummy" hole with using the standard tip produced marginal success as stress fractures were noted at the tip-to-well-pipe threaded joint.

Results for both PVC and reinforced fiberglass were identical, though the fiberglass has a much higher tensile strength (approximately 5 times that of PVC). The side-wall friction forces created tension; forces at the tip-case threaded joint were higher than either material could withstand. The tip-to-well joint failed in all trials with the standard tip. Note that these trials were made at a relatively "easy" site where CPT push forces were one-fourth to one-half of capacity.

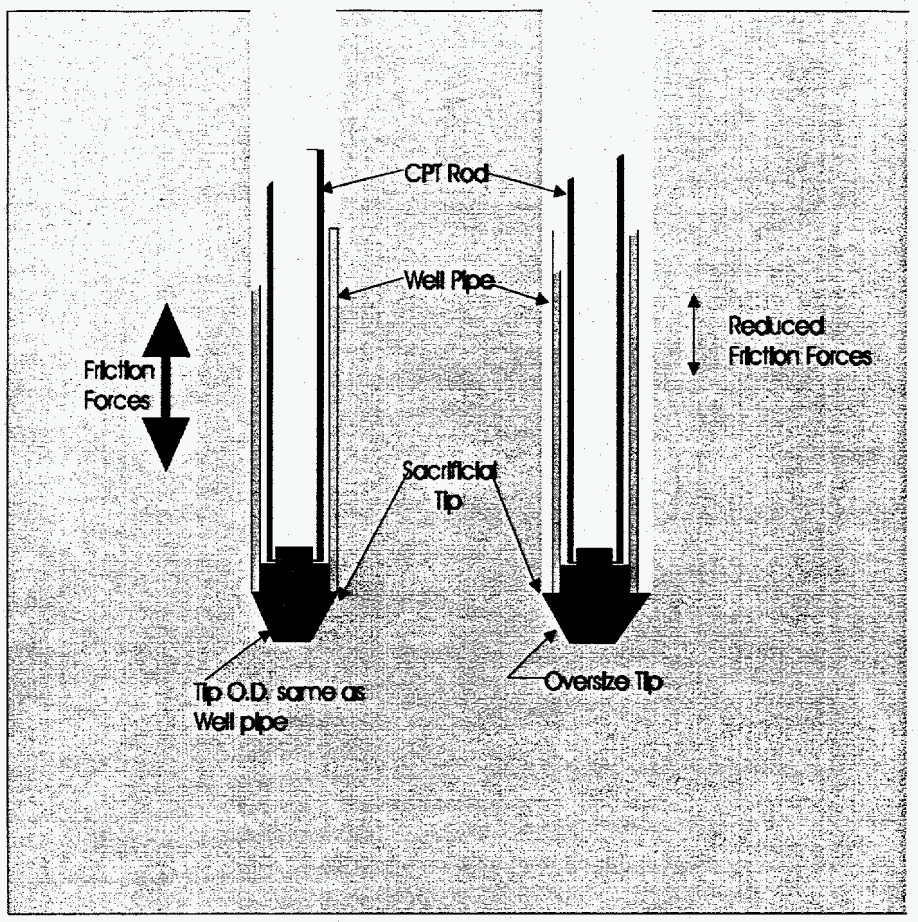

Figure 38 GeoWell installation test configurations with a standard and an oversized tip.

It was decided to do a standard CPT push at each well location while gathering CPT data, and then reoccupy these holes with the GeoWell using the oversize tip to insure successful installation. No particular difficulties were encountered during the GeoWell installations. However, there was concern that an air gap might exist between the electrode and the surrounding soil. It was thought that the soil would collapse quickly around the well making intimate electrical contact. Our field experience shows this is not always the case. Several possible solutions have been proposed including adding stainless steel fingers to the outside of the electrode and providing a means of adding water around the well to help collapse the hole. Figure 39 is a schematic of the GeoWell showing electrode spacing.

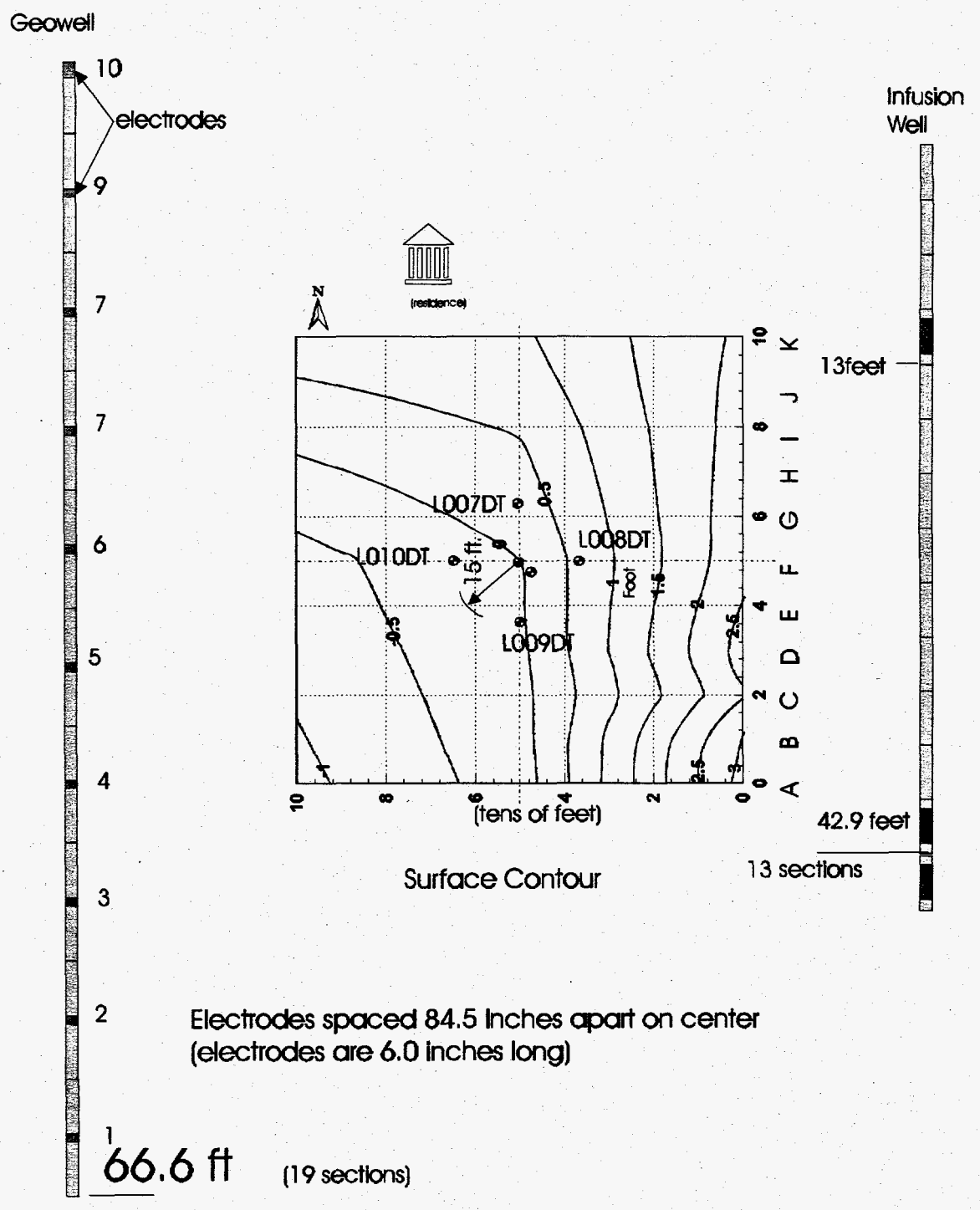

Figure 39. Dimensional schematic of the GeoWell, showing electrode numbering, and infiltration well.

4. GPR Borehole Antenna Testing in the GeoWell

The field test program envisioned using the same hole for both ERT and GPR. GPR borehole antennas were used in PVC-lined well casings and showed good results. However, the GeoWells had the addition of stainless-steel sections of threaded tubing, six inches long, spaced between PVC-threaded sections. The effect of a steel electrode on GPR borehole antenna tuning was not known. A scale mockup of two GeoWells, in air, was made in the laboratory. One set of borehole antennas was set up to operate with a 100MHz monocycle pulse; a digital oscilloscope was used to examine the received signal on the other antenna. Both antennas were moved along the GeoWell, past the electrodes, over their full length. The resulting signal on the oscilloscope showed no signal distortion and negligible amplitude change due to the SS electrodes.

It was concluded that the GeoWell's stainless steel electrodes have negligible effect on the radar signature. Further examination of the GPR tomographic images taken in the CPT installed GeoWells confirmed this conclusion.

B. BOREHOLE TEST RESULTS

The test program called for making cross-borehole measurements with both the ERT and GPR system from the same GeoWells before and after salt water infusion. The salt water infusion was designed to create a migrating plume to be imaged by the two techniques. The infusion depth was about 15 feet. The GeoWells had to be occupied sequentially by the electrode contactor strings and the GPR antennas. Each measurement set took several hours for both the ERT and GPR. The pre-infusion measurements were made over several days; however, the post-infusion measurements had to be made as quickly as possible to capture the migrating water plume.

1. Measurement Schedule

The following table shows the ERT GeoWell measurement schedule. The GPR measurements are interleaved with this schedule. Each ERT tomography experiment is controlled by an "Array Schedule File." This ERT measurement sequence is a list of all

combinations of 4 electrodes (2 for the transmitter and 2 for the receiver) which would be accessed during an experiment. Generally, all possible independent combinations of transmitter and receiver electrode pairs were used.

Table 3 Vermont Test Site ERT Measurement Schedule

Actual: Feb, 1997

Well	Pre Infusion	Post Infusion
1 to 3	2/12	2/17, 2/17, 2/18
2 to 4	2/12	2/17, 2/17, 2/19
1 to 4	2/12	2/17, 2/19
1 to 2	2/13	2/19
2 to 3	2/13	2/19
3 to 4	2/13	2/19

Resistivity data were taken several days before the salt water infusion process. Several sets were repeated to see if the data were repeatable and to determine the noise characteristics for the site, GeoWells, and ERT instrumentation. After a full suite of data were taken, the contactor strings were removed and GPR borehole data were taken in the same GeoWells. Based upon the good quality of the ERT images, it was decided to proceed with the salt water infiltration. As soon as the 100 gallons of water were injected through the infusion well, another set of GPR measurements were made. Because the GPR required a full day, additional resistivity data were taken the following day which yielded another set of images showing the progress or flow of the saline plume.

2. GPR Measurements

a) Transmit and Data Acquisition Settings:

Data was acquired using a time window of 750 nanoseconds (ns) over 1071 points (700 psec/pt). In order to improve signal to noise ratio, we averaged 64 consecutive received signals (64 stacks) for each transmitter-receiver position.

b) Cross-hole plane selection:

Four cross-hole scans were taken at the following GeoWells:

Transmitter	Receiver
4	1
1	2
4	2
1	3

Prior to making the tomographic measurements, a cross-hole scan was made wherein the transmitting and receiving antennas were kept at the same elevation and moved up the holes together. Figure 40 is an example of the received waveforms. The time and amplitude information of the "first arrival wavelet" was used in the 3DTOM software to create the tomographic images. Note the increase in travel time and decrease in amplitude between 20 and 30 feet. This was due to the wet clayey layers in that region (see Figure 37).

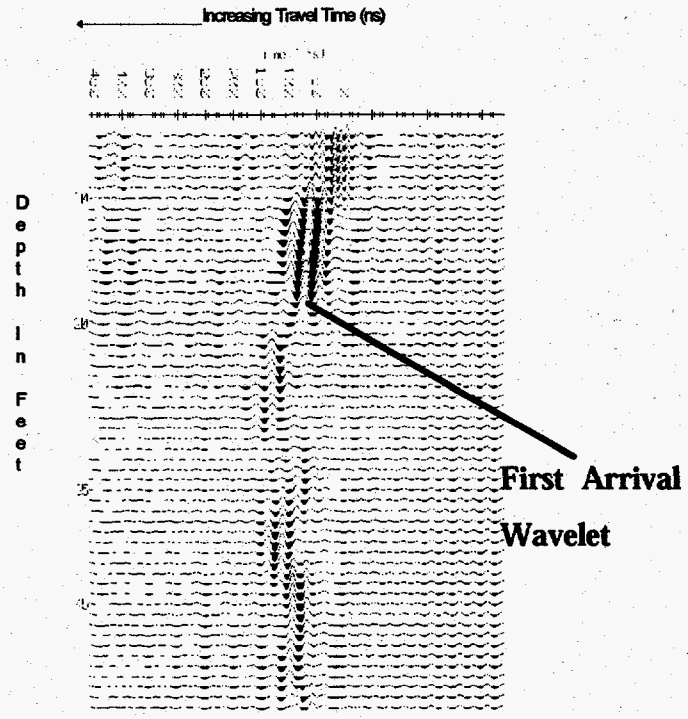

Figure 40. Example of GPR cross-hole data.

c) Antenna depth placements for tomographic measurements:

For each cross-hole scan, the transmitting antenna was placed at a depth from 10 feet to 50 feet. For each transmitter antenna position, the receiving antenna was placed at depths corresponding to the transmitter position plus and minus 20 feet in one or two foot increments (depending on desired resolution). The upper and lower limits of the receiving antenna were 5 feet and 60 feet respectively. After the receiver sequence was completed, the transmitting antenna was moved down one or two feet (depending upon desired resolution).

d) Air media calibration:

Before each cross-hole scan was performed, the two antennas were held above ground over the GeoWell. Approximately 10 transmit-receive wave forms were acquired and stored on disk.

e) Synchronization of antenna position with stored waveforms:

Each cross-hole scan sequence (for example the data acquired between holes 1 and 3) was stored on a separate computer file. For each sequence, a written chart was maintained to assure that each position was recorded. At preset intervals, usually the start of each new transmitter position, an electronic tic mark was placed on the data file. At the same time this position was marked on the chart.

f) Matlab Analysis:

Each raw data file was input to a software package (written in Matlab [31]) which performs the following operations:

1. Bandpass filter (butterworth) the data to remove any high frequency noise or low frequency trending.

2. Cosine taper the signal to give less weight to information at the edges of the scans where we do not expect to find valid signals.

3. Calculate the power envelope of the signal to give equal weight to positive and negative values.

4. Monitor and note the presence of an electronic tic mark.

5. Determine the time of arrival of the first signal maximum.

6. Compare the amplitude at the maximum to the average value of the power envelope.

7. Generate a new file storing the following parameters:

    1) Trace Number

    2) Tic mark presence flag

    3) First maximum onset time.

    4) Maximum vs. Average value flag

    5) Amplitude at the first maximum.

g) Correlation of processed signal trace with antenna position:

The file generated by the Matlab software was read into an Excel worksheet. Here, known electronic tic mark locations are lined-up with the tic mark flags on the data file. Data was then checked to see if resulting positions lined- up. Usually any discrepancy was due to a double acquisition at the point of electronic marking (easily observed by clearly similar values).

For each waveform, the maximum value vs. average amplitude flag was checked. If the value was zero, indicating that the maximum value was less than three times the average value, that waveform was removed from the set. For each cross-hole scan, the travel time values measured in air were determined (via the Matlab software). This value was subtracted from the raw time value recorded on the data file.

Finally, the data was reformatted to be read by our tomographic software (described below). The following 8 columns were stored to a new file:

1. A unique ID number for each waveform.
2. X coordinate of the transmitter
3. Y coordinate of the transmitter
4. Z coordinate of the transmitter
5. X coordinate of the receiver
6. Y coordinate of the receiver
7. Z coordinate of the receiver
8. Measured time at the position of the first maximum minus the air-wave time.

h) GPR Tomographic Imaging Software:

Antenna-pair position and arrival-time data as described above were input to Tomographic Imaging software 3DTOM beta version 1.0. This software, developed and provided by the U.S. Bureau of Mines, uses the simultaneous iterative reconstruction technique (SIRT) which repeatedly modifies an initial model to obtain the best possible fit to the data to a three-dimensional region.

3. ERT Results

The ERT data were processed using the LLNL software described earlier in Section IV. Figure 41 is an example of ERT images before and after the salt water infusion. The image resolution pixel size is about 2 feet. These results are very encouraging. The data above 25 feet did not pass the reciprocity test (see page 31) because the ground was too resistive. The blue areas are high resistivity and the red are low resistivity (see the Colormap Key of Log Resistivity). These areas correlate well with

the CPT logs where the sands have a higher resistivity than the clays, as would be expected. Note in the "after" image between 30 and 40 feet the major decrease in resistivity (red) due to the low resistivity salt water plume. Figure 42 includes the CPT soil classification logs for holes 1 and 3. The three clay zones (29 feet, 36-38 feet, and 50 feet) are represented by the yellow/red areas in the "before" ERT image. Being able to delineate between high and low resistivity layers is important, even though ERT does not have the resolution to map thin soil layers. Also being able to map resistivity changes for environmental monitoring purposes is an important result of this project.

Figure 43 shows the before and after ERT images for the plane between holes 1 and 4. Again note the changes in the region between 25 and 40 feet and three red zones in the "before" image that correlate with the clay layers. The saline plume seems to be centered at about 38 feet. The results in Figure 44, for the plane between holes 2 and 4, indicate that there was not much of a change due to the plume. Referring to the GeoWell site layout plan, Figure 32, and the discussion on expected plume flow direction, these results are consistent. The plume is moving in the northwesterly direction away from the plane between holes 2 and 4 and toward the plane between holes 1 and 4.

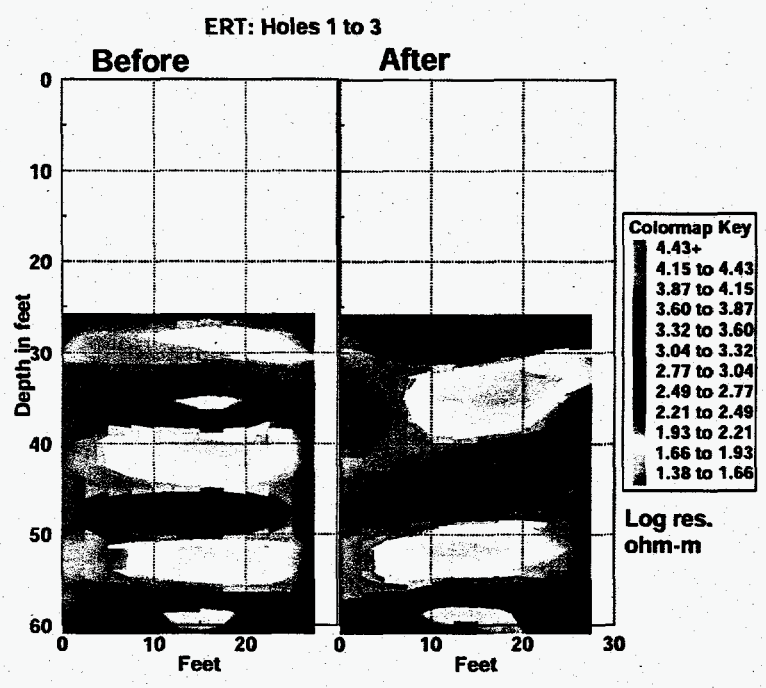

Figure 41. ERT tomographic images before and after salt water infusion for plane between holes 1 and 3.

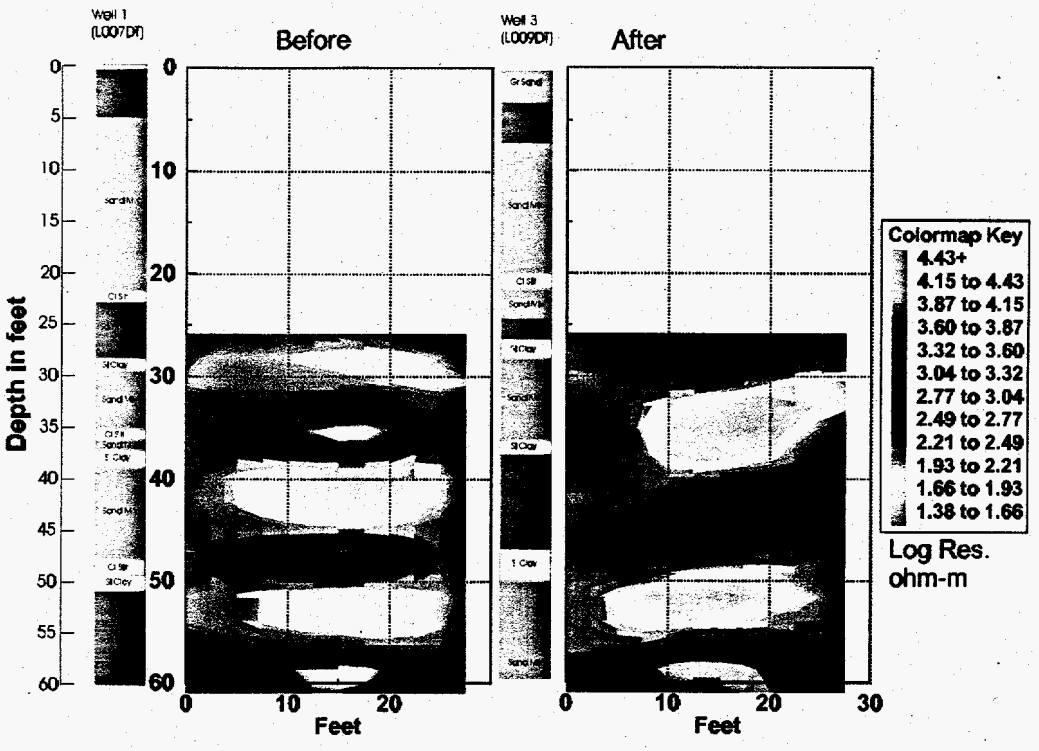

Figure 42. ERT images with CPT soil classification logs.

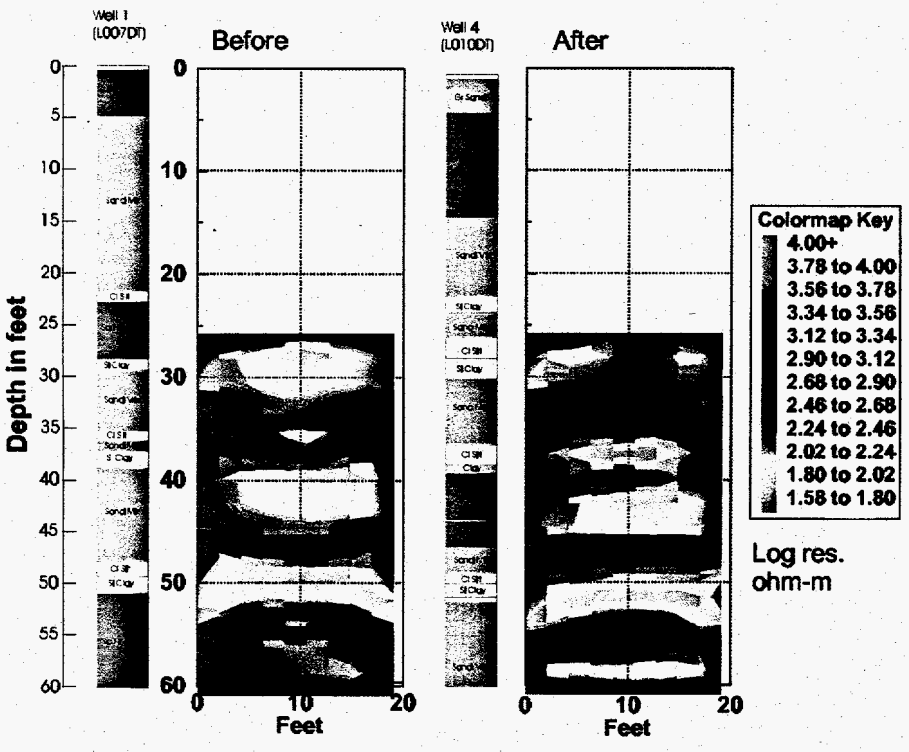

Figure 43. ERT images between holes 1 and 4.

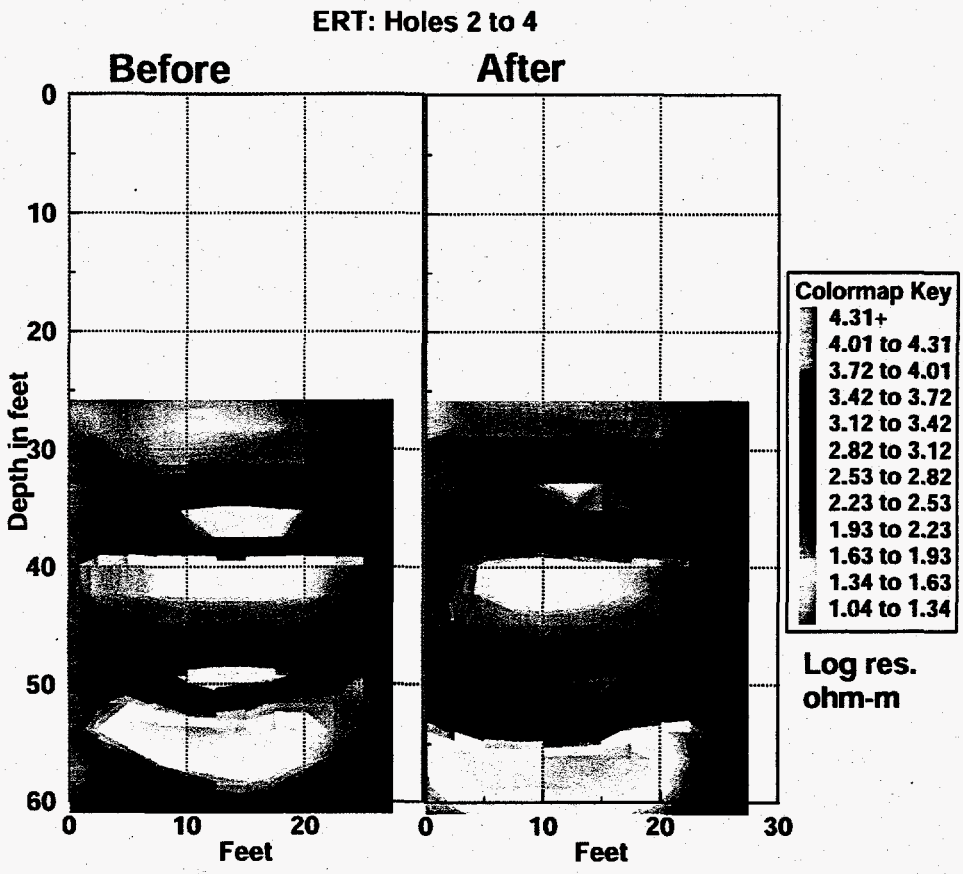

Figure 44. ERT image between holes 2 and 4.

4. GPR Results

The GPR data were processed using 3DTOM as described above. Figure 45 shows the before and after tomographic images for the plane between holes 1 and 4. For the GPR images the resolution pixel size is about 1.6 feet. The plume is quite evident in the "after" image. These GPR images are plots of radar signal velocity through the ground. Relatively high velocities, e.g. 0.4 feet/ns, represent dry or frozen sand, while low velocities, e.g. 0.1 feet/ns, are due to wet soils. Note the change in the region between 20 and 40 feet where the velocity has decreased (red/yellow) due to the increased water content from the water infiltration process.

There is not enough useful GPR data above a depth of 8 feet to properly image this region. The first transmitting antenna location starts at 10 feet with the receiving

antenna at 5 feet (this position is dictated by the 7-foot length of the antennas). Also the first arrival near the surface tends to be due to an "up-over-and-down" signal path through air (up the borehole, along the surface, and down the other borehole).

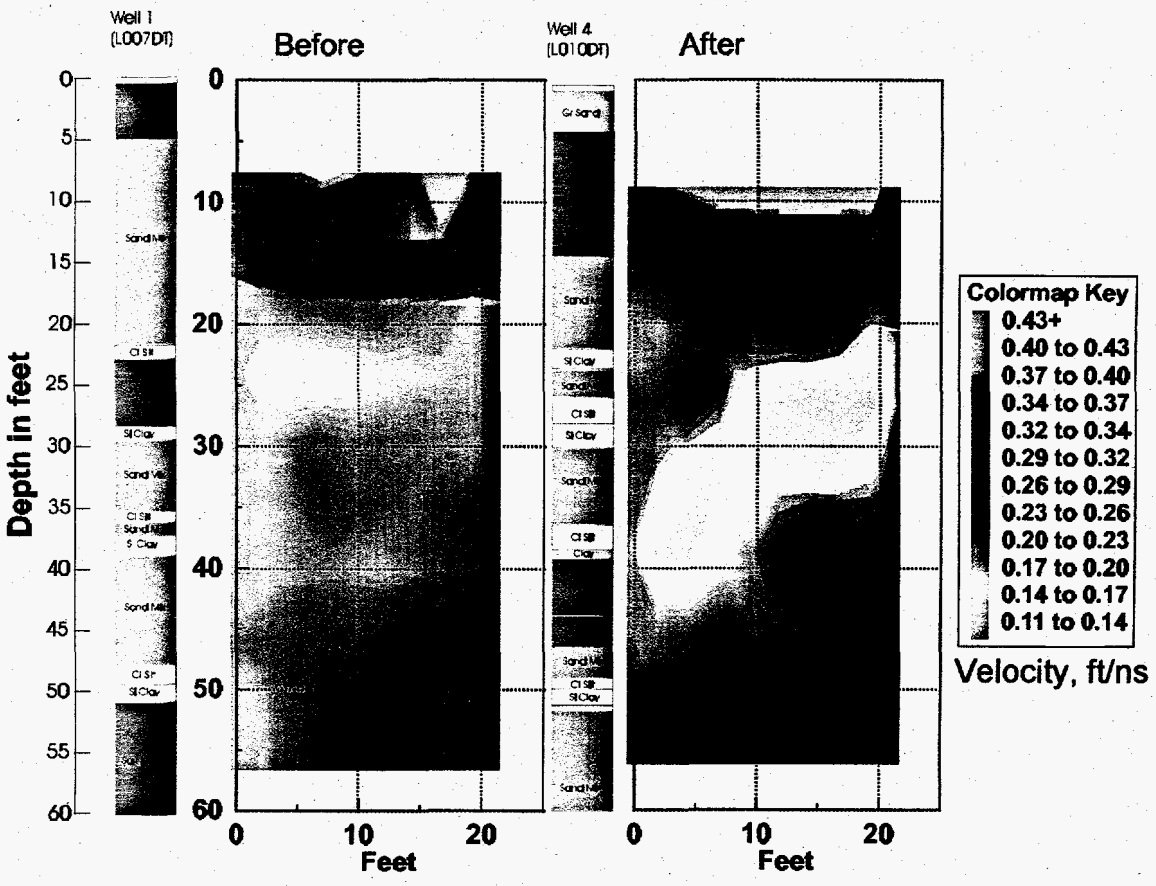

Figure 45. GPR tomographic images between holes 1 and 4.

Figure 46 is a comparison between ERT and GPR images. Even though the two methods respond to different electromagnetic soil properties, similar changes with depth are evident in the two images. The three wet clay regions are represented by low resistivity (red) areas in the ERT image and by the low velocity (red) areas in the GPR image. These results are consistent with the theory.

Note the lack of coverage above 25 feet in the ERT images and the coverage in this region in the GPR images. As explained earlier the soil was very resistive above 25 feet, limiting the amount of current injected into the ground, thus producing an

unacceptable signal-to-noise ratio for the ERT analysis. These ERT/GPR results demonstrate the value of combining two (or more) geophysical methods for site characterization and monitoring. ERT is more effective in *low* resistivity environments and GPR is more effective in *high* resistivity conditions.

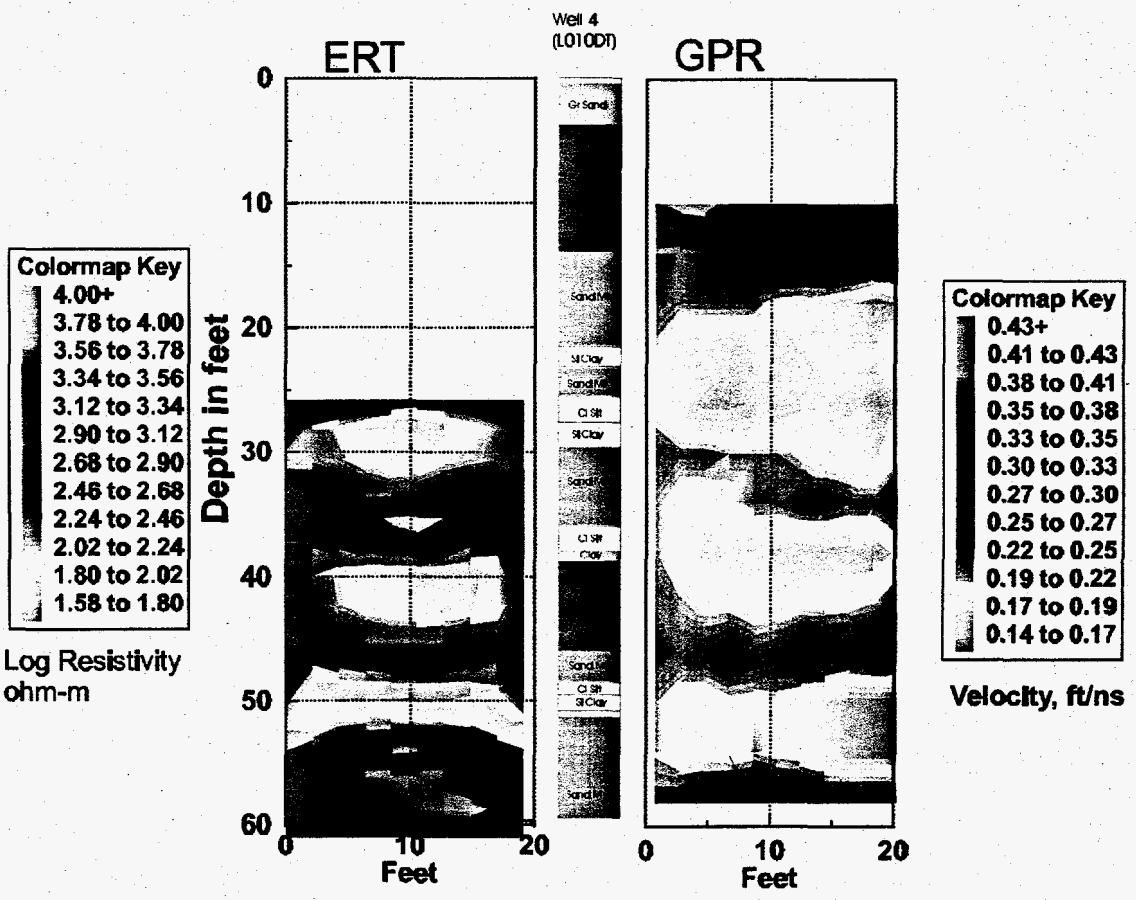

Figure 46. ERT and GPR comparison images between holes 1 and 4.

5. Soil Moisture Sensor (SMS) Results

The SMS was used to measure the soil moisture at the Monitoring Wells as a function of depth. Figure 47 is an example of a soil moisture log from Monitoring Well A compared with the CPT pore pressure log from GeoWell 4. The SMS results confirm that the clay layers are very wet. Where there was high pore pressure, e.g. at 22 and 28 feet,

the recorded moisture content was also high. Well constrictions prevented the SMS from going deeper than about 35 feet.

One purpose of using the SMS in the Monitoring Wells was to detect the presence of the water plume over time. However, for the SMS measurements that were made, there was no noticeable change with time. This may have been due to not logging deep enough (below 35 feet) or the sensitivity of the SMS instrument or the plume not intersecting the wells at the time of the measurements.

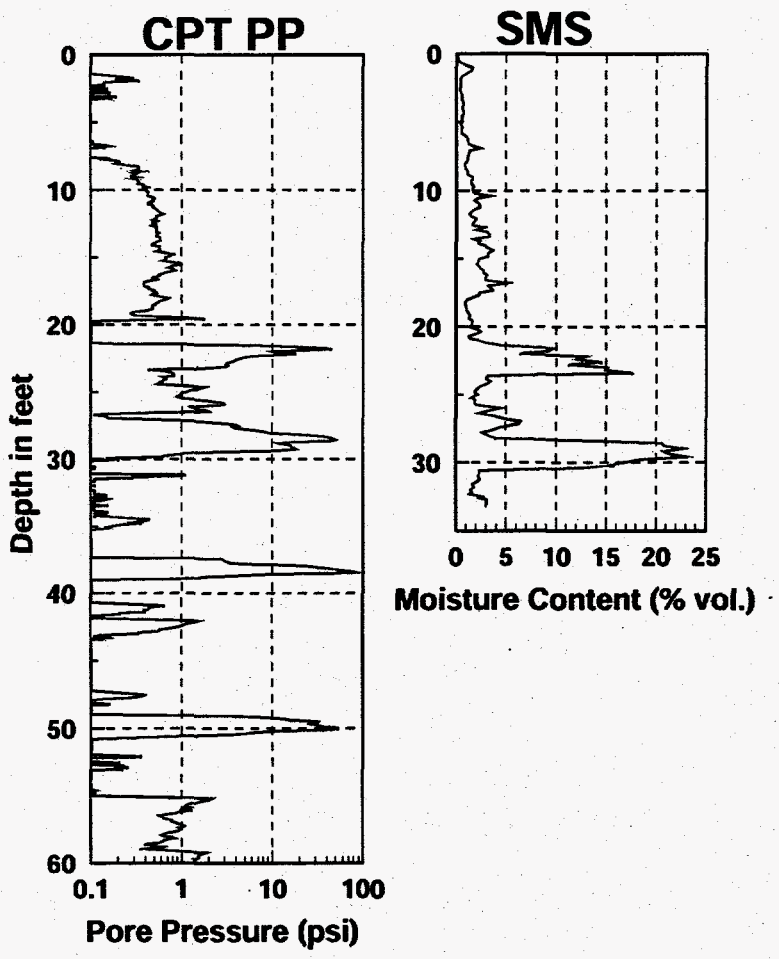

Figure 47. Pore pressure and SMS borehole logs.

SECTION VI.
CONCLUSIONS

Applied Research Associates is developing two new sensor packages for site characterization and monitoring. The two new methods are :

- Electrical Resistivity Tomography (ERT) and
- Ground Penetrating Radar (GPR) Tomography.

These sensor systems are now integrated with the Cone Penetrometer Technique (CPT). Surface ERT and GPR have proven to be useful techniques for imaging subsurface structures and processes; however, depth of investigation is limited. Borehole use of ERT and GPR require the installation of system components via drilled boreholes. The results of this program now make it possible to install ERT and GPR units by CPT methods and thereby reduce installation costs and total costs for ERT and GPR surveys. These two techniques can complement each other in regions of low resistivity where ERT is more effective and regions of high resistivity where GPR is more effective.

A breadboard ERT borehole system was built and successfully tested. A breadboard GPR borehole system was also built and successfully tested. CPT GeoWells were installed at ARA's Vermont Test Site for the field testing of the two cross-hole systems. A salt water infusion test at the site demonstrated the ability of the ERT and GPR techniques to image time variant processes. The pre-infusion and post-infusion tomographic images for both systems clearly show sand and clay layers and the water plume.

The results show that CPT-installed GeoWells can be used for both ERT and GPR borehole tomographic subsurface imaging. These two imaging techniques can be used for environmental site characterization and environmental remediation monitoring. Technologies used for site characterization and monitoring have numerous and diverse applications within site clean-up and waste management operations. DOE has identified a

need for sensors, sensor deployment means, and sensor data processing, including sensor data fusion methodologies for:

- detection and monitoring of contaminants in soils, groundwater, and process effluents;
- expediting site characterization; and
- geological and hydrogeological characterization and monitoring of the subsurface environment.

Our results specifically addresses each of these needs:

1. Sensors: Electrical Resistivity Tomography and Ground Penetrating Radar Tomography
2. Sensor Deployment: Cone Penetrometer Techniques
3. Sensor Data Processing: Tomographic Imaging
4. Sensor Data Fusion: ERT and GPR

Specific results are:

1. Delineating the continuity of soil layers between penetrometer holes;
2. Locating and mapping sand and clay lenses between penetrometer holes; and
3. Mapping plumes.

SECTION VII.
REFERENCES

1. J. D. Schroeder, S. R. Booth, and L. K. Trocki, "Cost Effectiveness of the Site Characterization and Analysis Penetrometer System," *LA-UR-91-4016*, Los Alamos National Laboratory, Los Alamos, NM, 1991.

2. S. R. Booth, C. J. Durepo, and D. L. Temper, "Cost Effectiveness of the Cone Penetrometer Technique (CPT)," *LA-UR-93-3383*, Los Alamos National Laboratory, Los Alamos, NM, 1993.

3. H. K. S. Begemann, "The Friction Jacket Cone as an Aid in Determining the Soil Profile," *Proc. 6th ICSMFE*, Montreal, vol. I, pp. 17-20, 1965.

4. J. de Reister, "Electric Penetrometer for Site Investigations," *Journal of SMFE Division,* ASCE, vol. 97, SM-2, Feb. pp 457-472, 1971.

5. B. A. Torstensson, "Pore Pressure Sounding Instrument," *Proc. ASCE Spec. Conf. on In Situ Measurement of Soil Properties*, Raleigh, NC, vol. II, pp. 48-54, 1975.

6. A. E. Z Wissa, R. T. Martin, and J. E. Garlanger, "The Piezometer Probe," *Proc. ASCE Spec. Conf. on In Situ Measurement of Soil Properties*, Raleigh, NC, vol. I, pp. 536-545, 1975.

7. D. A. Timian, B. E. Fisk, and B. R. Cassem, "Demonstration of Heavyweight Penetrometer Technology at the Hanford Site," *WHC-SD-TRP-003*, Westinghouse Hanford Company, Richland, Washington, Dec 1992.

8. W. Daily, A. Ramirez, D. LaBrecque, and J. Nitao, "Electrical Resitivity Tomography of Vadose Water Movement," *Water Resources Research*, vol. 28, pp. 1429-1442, May 1992.

9. A. Ramirez, W. Daily, D. LaBrecque, E. Owen, and D. Chesnut, "Monitoring an Underground Steam Injection Process Using Electrical Resistivity Tomography," *Water Resources Research*, vol. 29, pp. 73-87, Jan. 1993.

10. G. V. Keller and M. Frischknecht, *Electrical Methods in Geophysical Prospecting*, Pergamon, New York, 1966.

11. R. M. Morey, "Continuous Subsurface Profiling by Impulse Radar," *Proceedings of the Engineering Foundation Conference on Subsurface Exploration*, Henniker, NH; American Society of Civil Engineers, pp. 213-232, August, 1974.

12. R. M. Morey and W. S. Harrington, "Feasibility Study of Electromagnetic Subsurface Profiling", *Environmental Protection Technology Series EPA-R2-72-082*; US Environmental Protection Agency; October 1972.

13. D. J. Daniels, D. J. Gunton, and H. F. Scott, "Introduction to subsurface radar," *IEE Proceedings on Communication, Radar, and Signal Processing*, vol. 135, Pt. F, pp. 278-320, Aug. 1988.

14. K. Horton and R. M. Morey, "An Evaluation of Ground Penetrating Radar for Assessment of Low Level Nuclear Waste Disposal Sites", *Report NUREG/CR-2212*, U. S. Nuclear Regulatory Commission, September, 1981.

15. G. R. Olhoeft, "Geophysical Detection of Hydrocarbon and Organic Chemical Contamination," in Proc. *Symposium on the Application of Geophysics to Engineering and Environmental Problems*, pp 587-595, April 26-29, 1992, Chicago, IL.

16. K. A. Sander, G. R. Olhoeft, and J. E. Lucius, "Surface and Borehole Radar Monitoring of a DNAPL Spill in 3D versus Frequency, Look Angle and Time," in *Proc. Symposium on the Application of Geophysics to Engineering and Environmental Problems*, pp 455-469, April 26-29, 1992, Chicago, IL.

17. J. A. Bradley, and D. L. Wright, "Microprocessor-Based Data-Acquisition System for a Borehole Radar," *IEEE Trans. Geosci. Remote Sensing*, vol. GE-25, pp 441-447, 1987.

18. O. Olsson, L. Falk, O. Forslund, L. Lundmark, and E. Sandberg, "Crosshole investigation: Results from borehole radar investigations", *Stripa Project TR 87-11*, SKB, Stockholm, Sweden; 1987.

19. I. C. Peden, R. Kipp and J. Allestad, "A Scale-Model Study of Down-Hole VHF Dipole Arrays with Application to Subsurface Exploration", *IEEE Trans. Geosci. Remote Sensing*, vol. GE-30, pp 885-891, 1992.

20. R. Freedman and J. P. Vogiatzis, "Theory of microwave dielectric constant logging using the electromagnetic wave propagation method", *Geophysics*, vol. 44, pp 969-986, 1979.

21. G. S. Smith, "Directive Properties of Antennas for Transmission into a Material Half-Space," *IEEE Trans. on Antennas and Propagation*, vol. 32, pp 232-246, 1984.

22. D. L. Wright, R. D. Watts and E. Bramsoe, "A Short-Pulse Electromagnetic Transponder for Hole-to-Hole Use," *IEEE Trans. Geosci. Remote Sensing*, vol. GE-22, pp 720-725, 1984.

23. M. Sato and R. Thierbach, "Analysis of a Borehole Radar in Cross-Hole Mode," *IEEE Trans. Geosci. Remote Sensing*, vol. GE-29, pp 899-904, 1991.

24. A. H. Sihvola, "Self-Consistency Aspects of Dielectric Mixing Theories," *IEEE Trans. Geosci. Remote Sensing*, vol. GE-27, pp 403-415, 1989.

25. D. J. LaBrecque, G. Miletto, W. Daily, A. Ramirez, and E. Owen, "The Effects of Noise on Occam's Inversion of Resistivity Tomography Data", *Geophysics*, vol. 61, no. 2, pp. 538-548, 1996.

26. G. Miletto and D. J. LaBrecque, "Robust Scheme for ERT Inversion Modeling", in *Proc. Symposium on the Application of Geophysics to Engineering and Environmental Problems: EEGS*, Keystone, CO, pp. 629-638, April 28-May 2, 1996.

27. J. G. Maloney and G. S. Smith, "Optimization of a Conical Antenna for Pulse Radiation: An Efficient Design Using Resistive Loading," *IEEE Trans. on Antennas and Propagation*, vol. 41, pp 940-947, 1993.

28. T. T. Wu and R. W. P. King, "The Cylindrical Antenna with Nonreflecting Resistive Loading," *IEEE Trans. on Antennas and Propagation*, vol. 13, pp 369-373, 1965.

29. R. W. P. King and G. S. Smith, *Antennas in Matter*, The MIT Press, Cambridge, MA, 1981.

30. M. J. Jackson and D. R. Tweeton, "3DTOM: Three-Dimensional Geophysical Tomography," *Report of Investigations 9617*, US Department of the Interior, Washington, DC, 1996.

31. *MATLAB Reference Guide*, The MathWorks, Inc., 24 Prime Park Way, Natick, MA 01760, 1966.

SECTION VIII.

APPENDIX A

Vermont Test Site Field Logs

RADAN Filenames :

Vermont Site

GPR Surface Survey at 500 MHz

100 foot Square centered about infusion well

Data taken on 10 foot centers

0 trough 10 from Left to Right Facing away from house

A through K, A being further from house, outer LH corner

Grid Layout at Vermont Site
for GPR Surface Survey

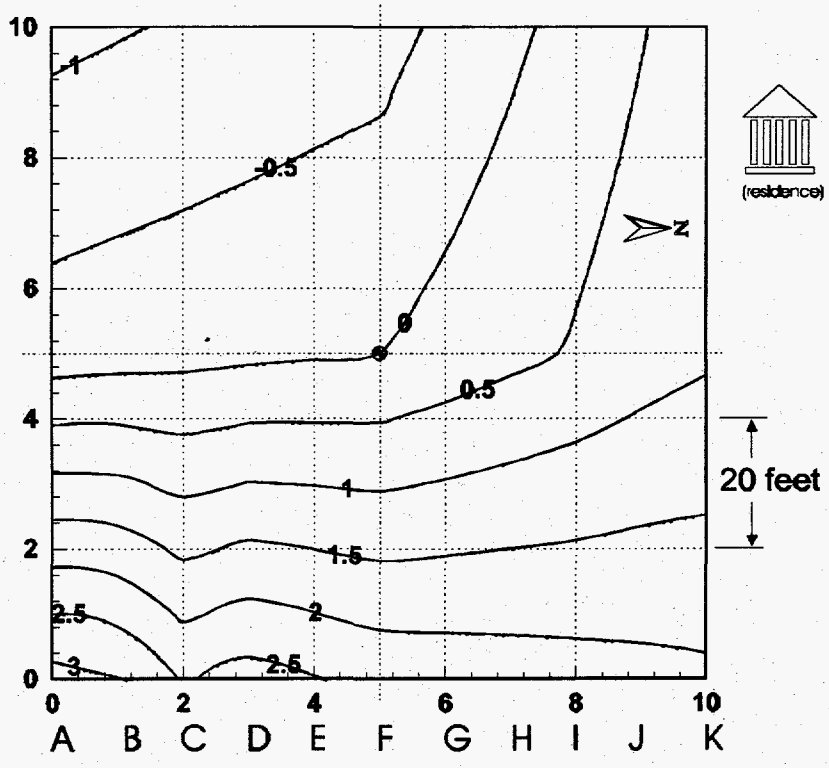

RADAN

Filename	Start	Stop
File52	D10	D0
File53	C0	C10
File54	B10	B0
File55	A0	A10
File56	E10	E0
File57	F0	F10
File58	A6	K6
File59	NONE	
File60	K7	A7
File61	A5	K5
File62	J10	J0
File63	J0	J10
File64	K10	K0
File65	I0	I10
File66	H10	H0
File67	G0	G10
File68	K10	A10
File69	A9	K0
File70	K8	A8
File71	NONE	
File72	A6	K6
File73	K4	A4
File74	A3	K3
File75	K2	A2
File76	A1	K1
File77	K0	A0

Surface topography data points:

Surface Topography		Feet
Datum F5	5.05	0.00
F0	2.70	2.35
A0	1.87	3.18
A5	5.31	-0.26
A10	6.18	-1.13
F10	5.74	-0.69
K10	4.26	0.79
K5	4.13	0.92
K0	2.96	2.09

Data array for surface contour map:

Surface Matrix in Feet

	0	1	2	3	4	5	6	7	8	9	10
A	3.18	2.49	1.80	1.12	0.43	-0.26	-0.43	-0.61	-0.78	-0.96	-1.13
B	3.01	2.37	1.73	1.08	0.44	-0.20	-0.37	-0.54	-0.70	-0.87	-1.04
C	2.45	1.93	1.41	0.89	0.37	-0.15	-0.31	-0.47	-0.63	-0.79	-0.95
D	2.68	2.12	1.57	1.01	0.46	-0.10	-0.25	-0.40	-0.56	-0.71	-0.86
E	2.52	2.01	1.49	0.98	0.46	-0.05	-0.19	-0.34	-0.48	-0.63	-0.77
F	2.35	1.88	1.41	0.94	0.47	0.00	-0.14	-0.28	-0.41	-0.55	-0.69
G	2.30	1.88	1.45	1.03	0.60	0.18	0.06	-0.05	-0.17	-0.28	-0.40
H	2.25	1.87	1.50	1.12	0.75	0.37	0.27	0.18	0.08	-0.01	-0.11
I	2.20	1.87	1.54	1.21	0.88	0.55	0.48	0.40	0.33	0.25	0.18
J	2.15	1.87	1.59	1.32	1.04	0.76	0.70	0.64	0.59	0.53	0.47
K	2.09	1.86	1.62	1.39	1.15	0.92	0.89	0.87	0.84	0.82	0.79

Data array for clayey-sand layer:

Layer 1 adjusted for surface features

	0	1	2	3	4	5	6	7	8	9	10
A	1.8352	1.1472	0.4592	-0.5568	-3.4096	-7.312	-10.4708	-11.9568	-13.1476	-14.0432	-14.2172
B	1.6652	1.0232	0.3812	-1.4744	-4.9372	-8.0392	-10.208	-12.3768	-14.152	-14.32	-16.1608
C	1.1052	0.5852	0.0652	-3.3412	-6.6164	-9.9572	-11.3636	-12.9668	-14.6684	-14.9596	-16.0708
D	1.3352	0.7792	-1.056	-5.1544	-8.2032	-10.7272	-13.5688	-14.8688	-15.5456	-16.4192	-17.3584
E	1.1752	0.6612	-3.3624	-6.4676	-10.6552	-11.4644	-14.3308	-14.6716	-15.4388	-16.6652	-16.8092
F	1.0052	0.5352	-3.2476	-6.8336	-9.9932	-12.2016	-13.2908	-14.6752	-15.5348	-16.1976	-17.09
G	0.9552	0.5312	-2.7792	-7.172	-12.188	-12.0872	-13.2528	-14.2216	-15.5184	-16.9464	-18.0136
H	0.9052	-0.3892	-4.8324	-7.242	-9.422	-11.9956	-11.862	-12.778	-14.3008	-16.3484	-16.9036
I	0.8552	0.1316	-3.5112	-9.0236	-12.5352	-10.8972	-12.9392	-14.6532	-16.3016	-16.8348	-18.1224
J	0.8052	0.5272	-4.6708	-8.36	-12.2788	-10.9496	-12.6148	-14.4112	-14.666	-15.6752	-16.5532
K	0.7452	0.5112	-3.3964	-7.632	-11.9988	-10.4944	-12.2588	-13.6624	-14.5084	-15.0264	-16.1676

Vermont Test Site

ERT Measurement Schedule

Actual: Feb, 1997

Well	Pre Infusion	Post Infusion
1 to 3	2/12	2/17, 2/17, 2/18
2 to 4	2/12	2/17, 2/17, 2/19
1 to 4	2/12	2/17, 2/19
1 to 2	2/13	2/19
2 to 3	2/13	2/19
3 to 4	2/13	2/19

SECTION IX.

APPENDIX B

CPT Logs from Vermont Test Site

INF APPLIED RESEARCH ASSOCIATES, INC. 12/08/96

INFILTRATION WELL

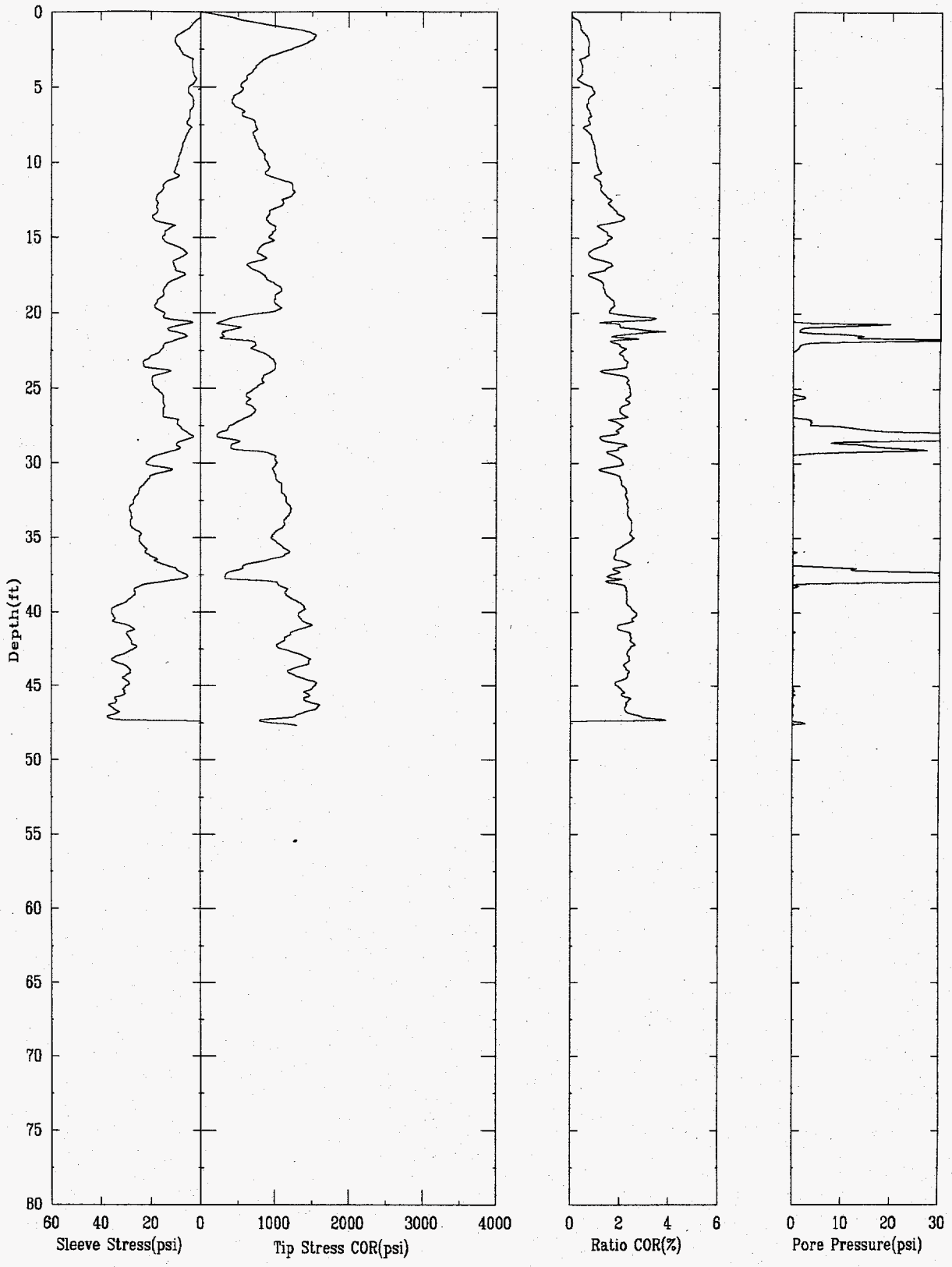

File 508d601.ECP

INF APPLIED RESEARCH ASSOCIATES, INC. 12/08/96

INFILTRATION WELL (cont.)

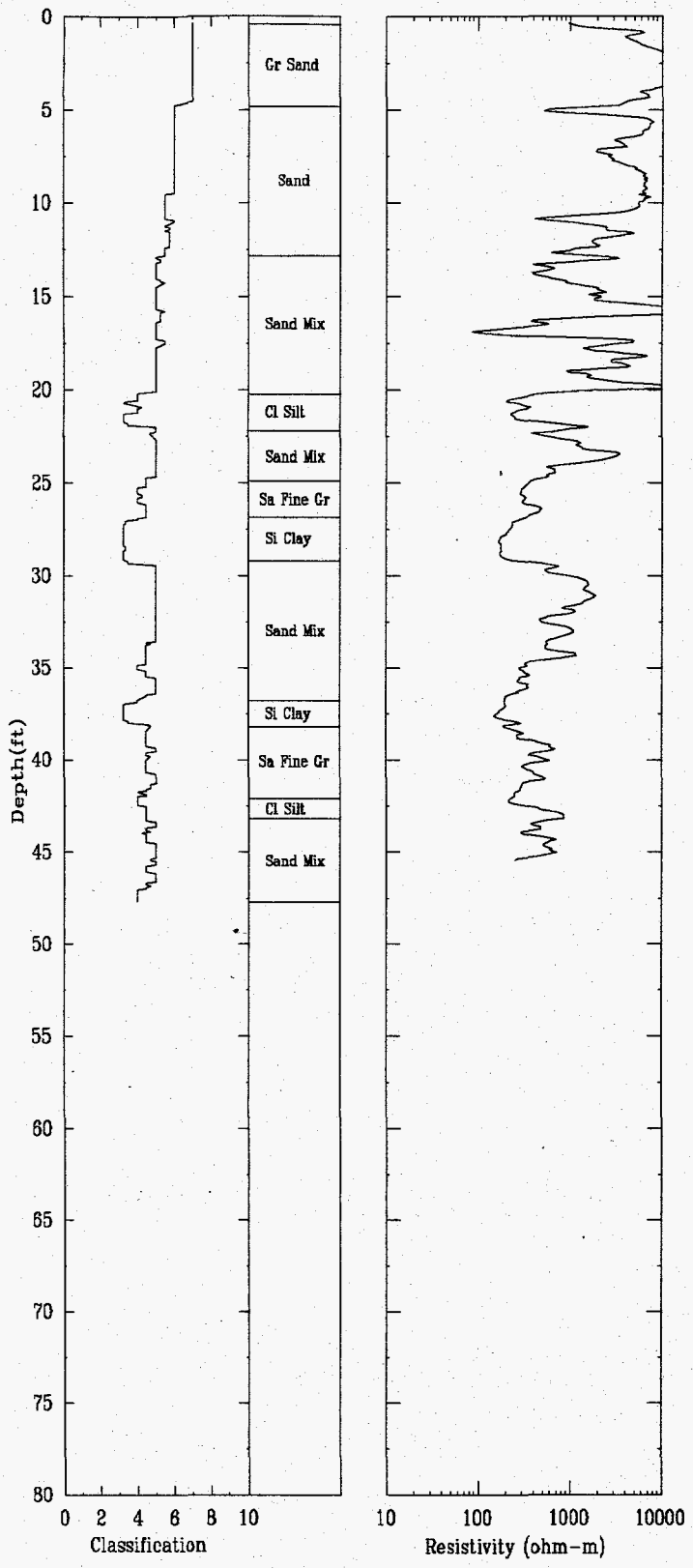

File 508d601.ECP

L007DT APPLIED RESEARCH ASSOCIATES, INC. 11/22/96

GEOWELL 1

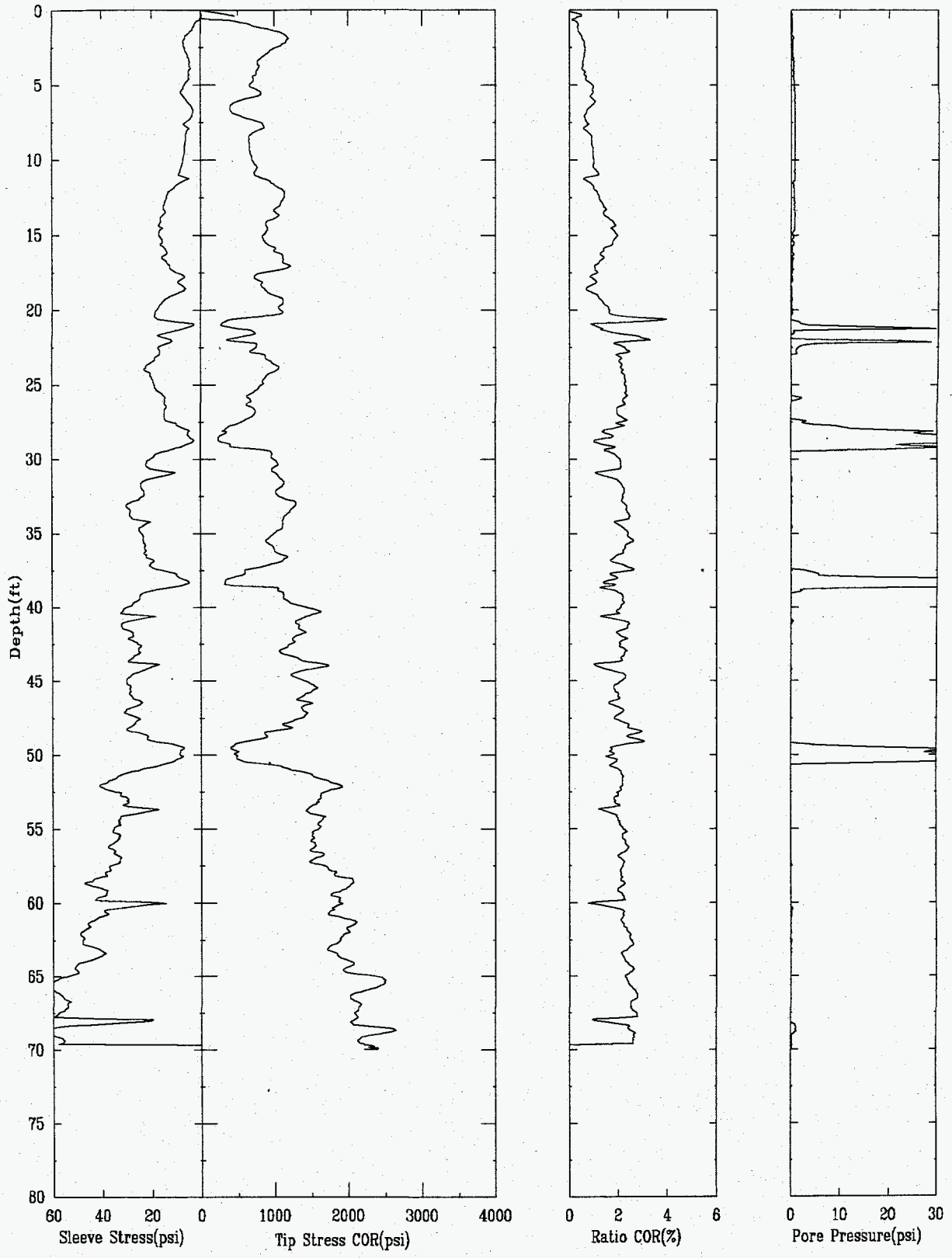

File 522n605.ECP

L007DT APPLIED RESEARCH ASSOCIATES, INC. 11/22/96

GEOWELL 1 (cont.)

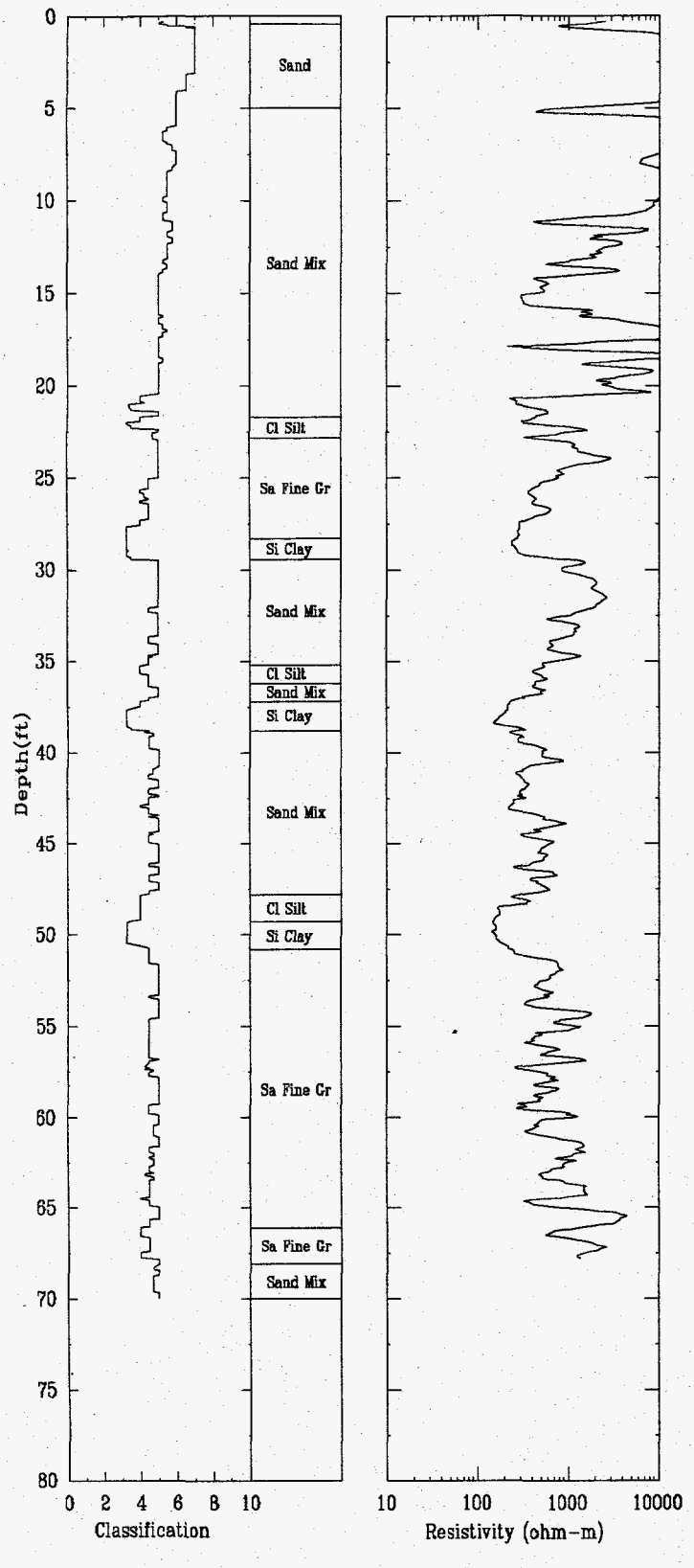

File 522n605.ECP

L008DT APPLIED RESEARCH ASSOCIATES, INC. 11/25/96

GEOWELL 2

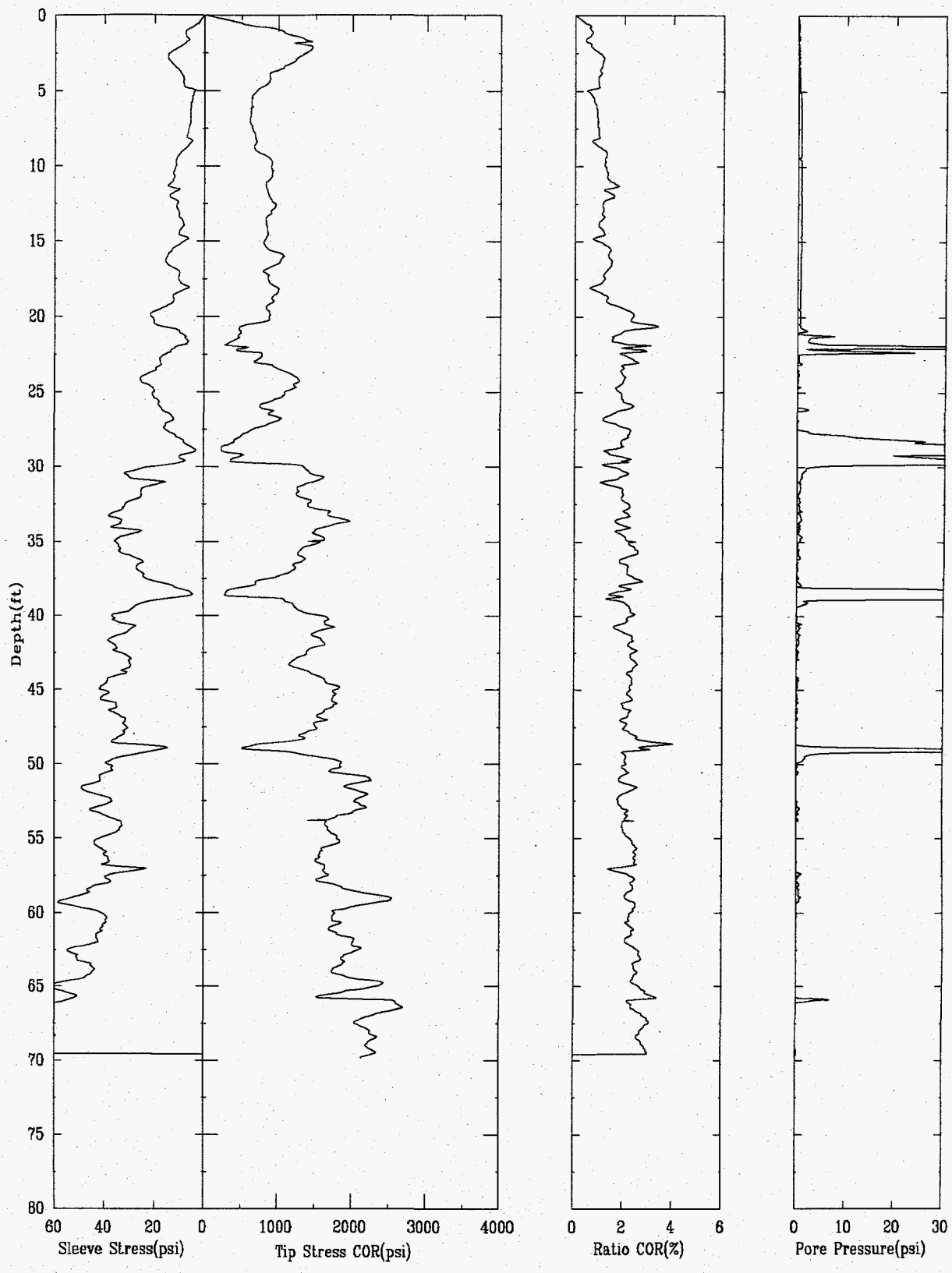

File 525n602.ECP

L008DT APPLIED RESEARCH ASSOCIATES, INC. 11/25/96

GEOWELL 2 (cont.)

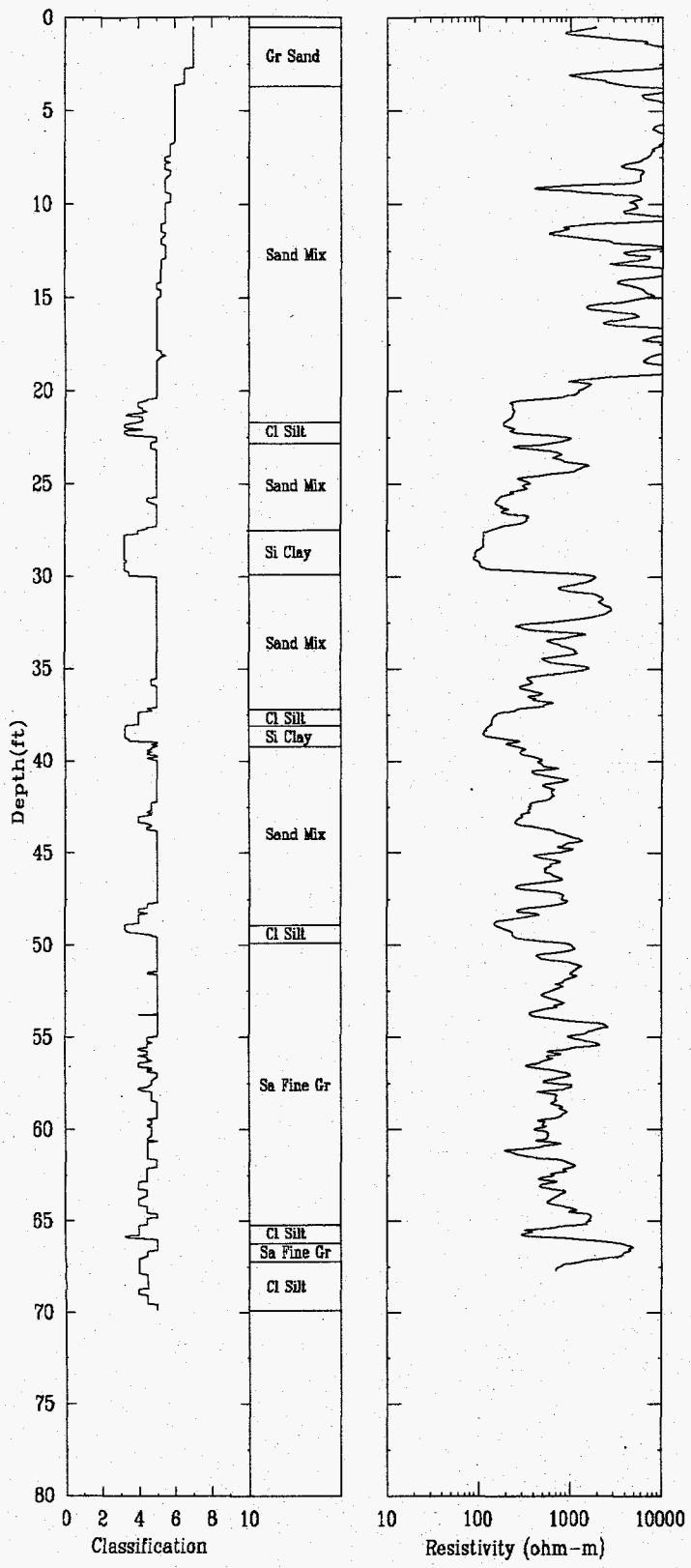

File 525n602.ECP

L009DT APPLIED RESEARCH ASSOCIATES, INC. 12/07/96

GEOWELL 3

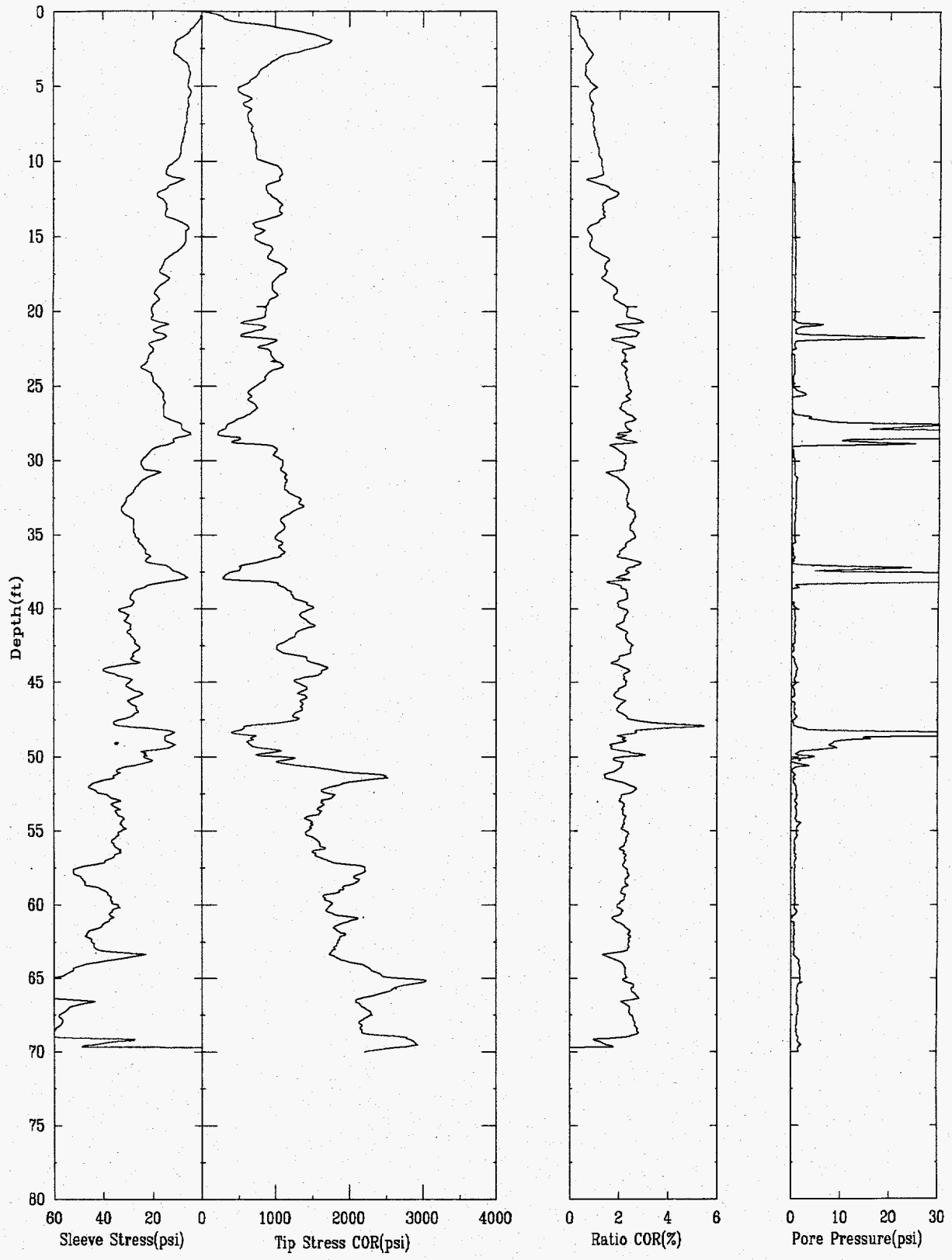

File 507d603.ECP

GEOWELL 3 (cont.)

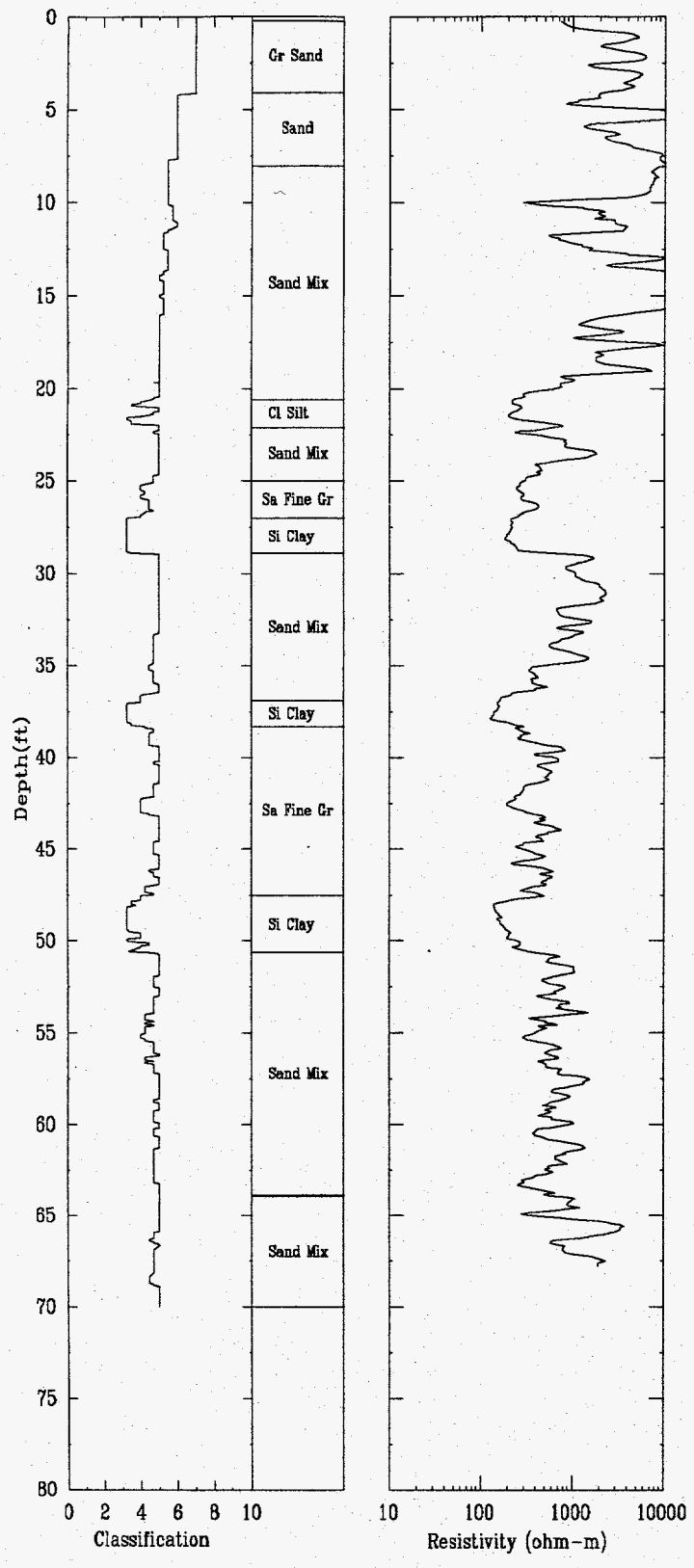

File 507d603.ECP

L010DT APPLIED RESEARCH ASSOCIATES, INC. 12/08/96

GEOWELL 4

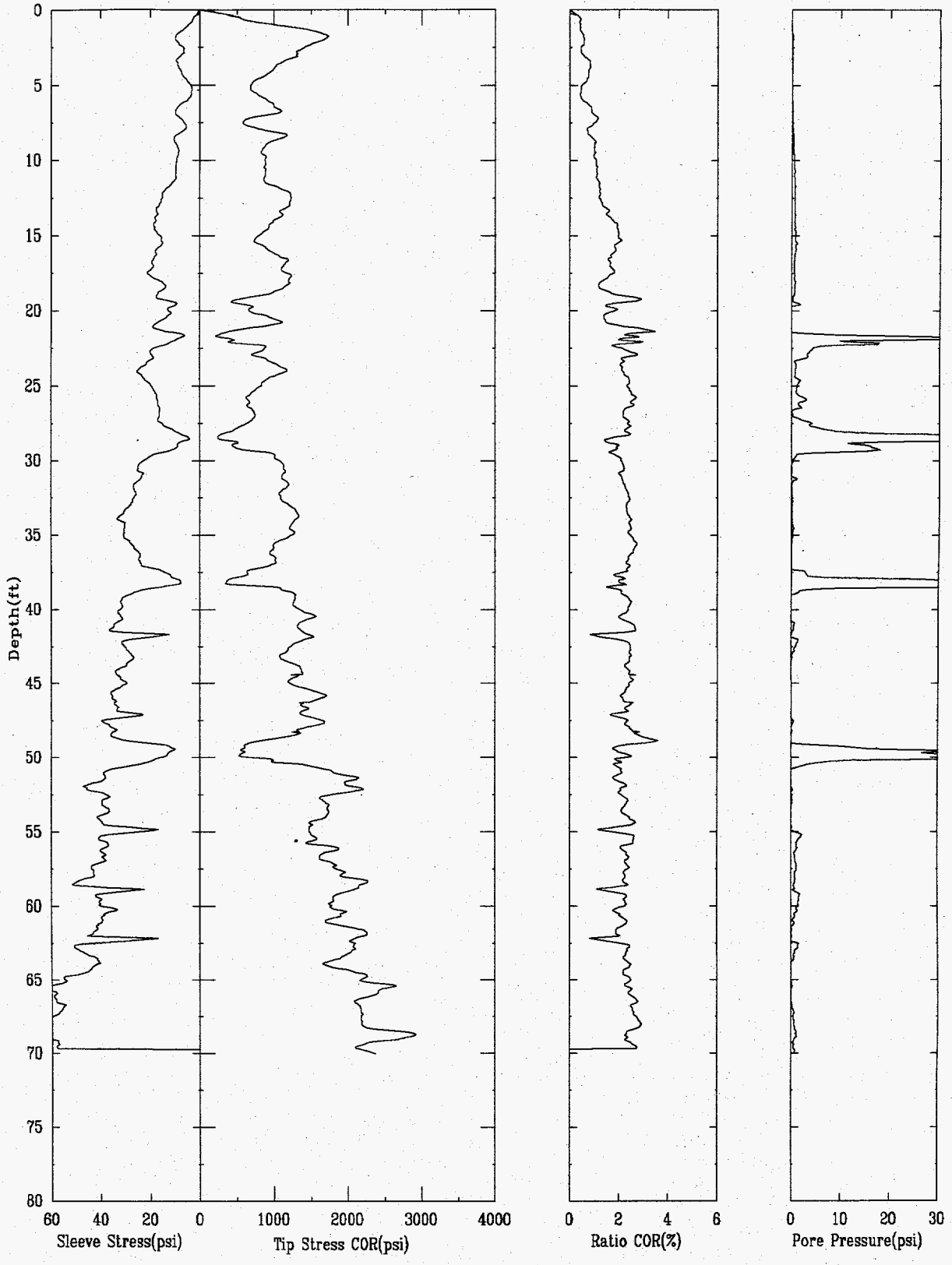

File 508d604.ECP

GEOWELL 4 (cont.)

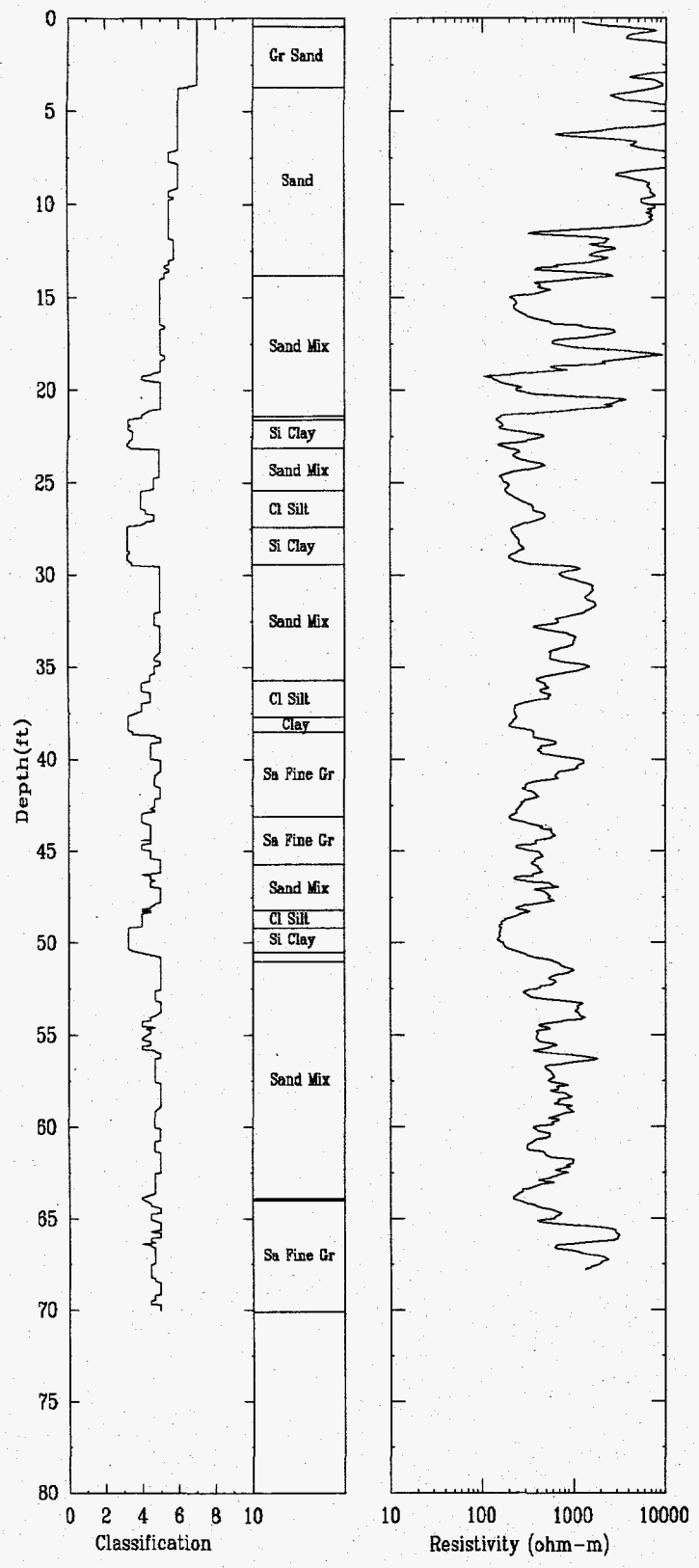

File 508d604.ECP